# A new mineral from the Bellerberg, Eifel, Germany, intermediate between mullite and sillimanite.

Reinhard X. Fischer[1], Valeria Tikhonova[1], Johannes Birkenstock[1], Lennart A. Fischer[2], Klaus Herrmann[3], Kurt Mengel[3], and Hartmut Schneider[1,4]

[1]Fachbereich Geowissenschaften, Universität Bremen, Klagenfurter Straße, D-28359 Bremen, Germany, e-mail rfischer@uni-bremen.de

[2]Institut für Mineralogie, Leibniz Universität Hannover, Callinstraße 3, D-30167 Hannover, Germany

[3]Institut für Endlagerforschung, TU Clausthal, Adolph-Roemer-Straße 2A, D-38678 Clausthal-Zellerfeld, Germany

[4]Institut für Kristallographie, Universität zu Köln, Greinstraße 6 D-50939 Köln, Germany

Corresponding author: Reinhard X. Fischer
Fachbereich Geowissenschaften
der Universität
Klagenfurter Straße
D-28359 Bremen
Germany
Tel. (421) 218-65160
FAX (421) 218-65189
e-mail: rfischer@uni-bremen.de

**ABSTRACT**

A mineral intermediate between sillimanite and mullite, tentatively designated as „sillimullite“, was studied by electron microprobe analyses and single-crystal X-ray diffraction methods. The chemical compositions derived from the microprobe results and the crystal-structure refinement are $Al_{7.84}Fe_{0.18}Ti_{0.03}Mg_{0.03}Si_{3.92}O_{19.96}$ and $Al_{8.28}Fe_{0.20}Si_{3.52}O_{19.76}$ (Fe is $Fe^{3+}$) corresponding to *x*-values of 0.02 and 0.12, respectively, in the solid-solution series $Al_{8+4x}Si_{4-4x}O_{20-2x}$ assigning $Fe^{3+}$, Ti, and Mg to the Al site. The composition derived from microprobe analysis is very close to a stoichiometric sillimanite (with $Fe^{3+}$,Ti, and Mg assigned to Al sites) while the composition derived from diffraction data is midway between sillimanite and Si-rich mullites. The discrepancy is assumed to be caused by the occurrence of amorphous nano-sized $SiO_2$ inclusions in the aluminosilicate phase not affecting the diffraction data but detected in the microprobe analysis. „Sillimullite“ crystallizes in the orthorhombic space group *Pnam* with $a = 7.5127(4)$ Å, $b = 7.6823(4)$ Å, $c = 5.785(3)$ Å, V = 333.88(4) Å$^3$, $Z = 1$. It has a complete Si/Al ordering at tetrahedral sites like sillimanite but with neighboring double chains of $SiO_4$ and $AlO_4$ tetrahedra being offset by ½ unit cell parallel to **c** relative to each other causing the change of the space-group setting from *Pbnm* (sillimanite) to *Pnam*. Difference Fourier calculations and refinements with anisotropic displacement parameters revealed the formation of oxygen vacancies and triclusters as known in the crystal structures of mullite. Final refinements converged at R1 = 5.9% for 1024 unique reflections with $F_o > 4\sigma(F_o)$. Fe was found to reside predominantly in the octahedral site and with minor amounts in one of the T* sites. Mg and Ti were not considered in the refinements. The crystal studied here is considered to represent a new mineral intermediate between sillimanite and mullite, named „sillimullite“.

## INTRODUCTION

Burnham (1964) mentioned that the mullite structure theoretically fits to any composition between $x = 0$ and $x = 1$ with respect to the general formula $Al_{4+2x}Si_{2-2x}O_{10-x}$. The main compounds are sillimanite ($x = 0$), 3/2-mullite ($x = 0.25$) and 2/1-mullite ($x = 0.4$, see, e.g., Fischer and Schneider, 2005). Alumina with a hypothetical mullite-type structure (ι-alumina, $x = 1$) was described by Perrotta and Young (1974) but most probably contains alkaline elements as discussed by Fischer and Schneider (2005). More recently, Ebadzadeh and Sharifi (2008) published data on the synthesis of pure ι-alumina, but structural details were not given. Numerous studies in this research field have shown that the situation is complicated. Synthetic mullites normally have compositions $0.25 \leq x \leq 0.40$ where the lower $x$-value corresponds to 60 mol% $Al_2O_3$ (3/2-mullite, $3Al_2O_3 \square 2SiO_2$, $x = 0.25$), and the upper $x$-value to 66.7 mol% $Al_2O_3$ (2/1-mullite, $2Al_2O_3 \square SiO_2$, $x = 0.40$). 3/2-mullites have been designated as “sinter-mullites”, since they are often formed by solid-state reactions. 2/1-mullites usually grown from melts are termed “fused-mullites”. Compounds intermediate in composition between 3/2 and 2/1 mullite are formed by sol-gel based processes and by annealing 3/2-mullites at temperatures $> 1600$°C. Schneider et al. (1993) described an $Al_2O_3$-rich phase with $x = 0.83$ (89 mol% $Al_2O_3$), which was prepared using specific sol-gel routes. However, increasing $Al_2O_3$ content destabilizes the mullite structure. This especially comes true at $Al_2O_3$ contents > 80 mol% ($x = 0.67$). In this composition range the tetrahedral triclusters, being typical for mullite, are gradually replaced by tetrahedral tetraclusters, where 4 tetrahedra are connected by a bridging oxygen atom instead of 3 in the case of the triclusters. At the $SiO_2$-rich side of the $Al_2O_3$ - $SiO_2$ system at $x < 0.25$ a miscibility gap towards sillimanite ($x = 0$) is assumed under ambient pressure. The occurrence of the miscibility gap can be explained by the different ordering schemes of sillimanite and mullite. On the other hand, the question whether phases with compositions between sillimanite ($x = 0$)

and 3/2-mullite ($x = 0.25$) exist is still controversial. A continuous isomorphic series between sillimanite and 3/2-mullite was proposed by Ďurovič (1962) and Hariya et al. (1969). On the basis of high-temperature and high-pressure experiments they demonstrated that compositions between sillimanite and mullite can be achieved by varying the pressure and temperature conditions in the synthesis process. However, Hariya et al. (1969) gave no information on the crystal structures of theses phases. On the other hand, Cameron (1976a) interpreted the coexistence of sillimanite and mullite in natural rocks as an evidence for the presence of a miscibility gap between the two phases. Further on, Cameron (1976b) described a naturally occurring mineral phase intermediate in composition between sillimanite and mullite. This, however, contained an appreciable amount of Fe, and it was suspected that iron might stabilize this compound. In a subsequent work he states "If Ti is absent, $Fe^{3+}$ can stabilize the Si-Al ordering scheme characteristic of 1:1 sillimanite to well into the previously known mullite composition range" (Cameron 1977).

Although natural mullites, mullite-type alumino silicates with compositions midway between sillimanite and 3/2-mullite (Cameron, 1976), and phases approaching sillimanite in composition can be found in nature (e.g. Fischer and Schneider, 2005), no structure refinement data are available so far. This is surprising since there is no paucity of suitable specimens. The present study intends to fill this gap by providing data on a mineral which has a composition intermediate between sillimanite and Si-rich mullite, but which has a crystal structure distinctly different from both. A proposal on this mineral has been submitted to the IMA commission for new minerals just recently. Therefore, the name "sillimullite" is not approved yet, but used here as a tentative name for this species.

## EXPERIMENTAL

The “sillimullite” crystal (slightly pink color, acicular habit, approximately 0.2×0.02×0.02 $mm^3$) was separated from a rock sample collected in the basalt quarry Caspar at the Ettringer Bellerberg near Mayen (Eifel area, Germany). The crystal was mounted on a Bruker D8 Venture single-crystal diffractometer with Mo-$K_{\alpha1}$-$K_{\alpha2}$ radiation (classic tube at 50 kV, 30 mA) equipped with a curved Triumph monochromator, a 0.6 mm collimator, a four-circle diffractometer (kappa geometry) and a Photon 100 CMOS area detector (Fachbereich Geowissenschaften, University of Bremen). Data collection parameters and crystal data are listed in Table 1. After data collection, the crystal was prepared for electron microprobe analyses using two different Cameca instruments at Universities of Hannover and Clausthal to ensure the reproducibility of the results. Instrumental parameters and setups for both instruments are listed in Table 2. At Leibniz Universität Hannover, the Cameca SX100 microprobe was equipped with five spectrometers having a static (fixed) beam. Standards were wollastonite for Si, corundum for Al, rutile for Ti, hematite for Fe, and periclase for Mg. The Cameca SX100 at TU Clausthal had four spectrometers. Pyrope was used as a standard for Si, Al, Fe, Mg, and Ti, boron nitride and a borosilicate glass (DURAN®) for B. Both instruments were operated with an acceleration voltage of 15 kV and a beam current of 15 nA with a counting time of 10 s. The matrix correction PAP was done after Pouchou and Pichoir (1991). Upon preparation the polished crystal split parallel to its long **c** axis into two main parts. One of the two parts was slightly tilted relative to the plane of preparation and thus yielded inaccurate signals. This was checked by rotating the sample by 180° to confirm that the difference in the detected intensity was due to the effect of the tilt on the instrument and not to differences in chemical composition between the left and right parts of the crystal. Turning the sample is equivalent to switching opposite spectrometers of the microprobe, each of them being sensitive for either Si or Al analyses. Therefore, the signals from the tilted half are different for opposite spectrometers and the results from the left part of the crystal (Fig. 1)

were excluded from calculating the average composition. Results are given in Table 2 corresponding to the analyzed spots shown in Fig. 1 yielding the average composition of 61.2(5) wt% $Al_2O_3$, 36.1(4) wt% of $SiO_2$, 2.2(2) wt% $Fe_2O_3$, 0.3(1) wt% $TiO_2$, and 0.21(4) wt% MgO corresponding to 49.0(4) mol% $Al_2O_3$, 49.1(5) mol% $SiO_2$, 1.1(1) mol% $Fe_2O_3$, 0.35(12) mol% $TiO_2$, and 0.42(8) mol% MgO. The resulting atomic compositions per unit cell are listed in Table 2b. This corresponds to a normalization of the atomic composition to 12 cations. Assuming that all Fe is $Fe^{3+}$ replacing Al together with Ti and Mg this yields a chemical composition of $Al_{7.84(5)}Fe_{0.180(17)}Ti_{0.028(10)}Mg_{0.033(6)}Si_{3.92(4)}O_{19.96(2)}$ based on the standard mullite composition with doubled unit cell volume $(Al,Fe)_{8+4x}Si_{4-4x}O_{20-2x}$ corresponding to an *x*-value of 0.02.

Great care was bestowed on the detection of boron in “sillimullite”. Boron is an essential constituent of grandidierite (Dzikowski et al., 2007), a mineral related to mullite that is reported intergrown with it at the Bellerberg (Blaß and Graf, 1994). Even sillimanite has been reported to contain small amounts of boron (Grew and Hinthorne, 1983; Grew and Rossman, 1985). However, no boron could be found within the detection limits (< 0.3 wt. %) of the electron microprobe using the Cameca PC3 ($Mo/B_4C$ multilayer) spectrometer.

A careful analysis of systematic absences of reflections was done with the crystallographic computing system Jana2006 (Petříček et al. 2006). The program SHELXL-97 (Sheldrick 1997; Sheldrick 2008) as part of the WINGX suite (Farrugia 1999) was used for the crystal-structure refinements. Crystal structure projections were drawn with the program STRUPLO (Fischer and Messner 2013).

## RESULTS

The inspection of layers in reciprocal space immediately revealed the superstructure reflections causing the doubling of the *c* lattice parameter of „sillimullite“ with respect to the

155 standard mullite unit cell resembling the metrical parameters of sillimanite. Fig. 2 shows a
156 characteristic layer calculated from the observed intensities. It was carefully checked that the
157 superstructure reflections are not caused by λ/2-effects of the X-ray beam: If they were
158 caused by this effect the intensity ratios between superstructure reflections *hkl* (with l=2n+1)
159 and the respective *2h2k2l* reflections would exhibit a constant value. This was not the case
160 and in some cases the intensity of the superstructure reflection was even stronger than that of
161 the respective *2h2k2l* reflection. Furthermore for strong *hkl* reflections we did not observe any
162 λ/2 reflections *h/2 k/2 l/2* at positions that are not imposed by the *2**c*** superstructure (e.g., in
163 the *hk0* layer).

164 The orthorhombic unit cell was chosen to conform to a setting with lattice parameters *a* <
165 *b* representing the usual setting known for sillimanite and mullite. In this setting, the
166 evaluation of the intensities with Jana (Petříček et al. 2006) revealed a clear preference for
167 space group setting *Pnam*, rather than *Pbnm*, the latter corresponding to the standard setting
168 of sillimanite. In the *Pbnm* setting 186 systematic absence violations of reflections with $I > 4\sigma$
169 were found while none are present in the *Pnam* setting. Alternatively, space-group setting
170 *Pbnm* could be achieved if basis vectors **a** and **b** were interchanged. But this would not fit to
171 the normal evolution of the lattice parameters on the silica rich part of the diagram in Fig. 3
172 with *b* > *a*. Therefore, space-group setting *Pnam* was used for the description of the crystal
173 structure. Structural relationships between the two settings are discussed in the general
174 description paragraph of the discussion section.
175 Subsequently, atom positions were generated by transforming the coordinates of sillimanite
176 (Yang et al. 1997) to *Pnam*. At this stage, a pure $Al_2SiO_5$ sillimanite composition was
177 assumed ignoring Fe, Mg, and Ti. Refinement with isotropic displacement parameters
178 converged at R1=13.4% for 1024 reflections with $F_o > 4\sigma(F_o)$. Difference Fourier calculations
179 immediately revealed maxima of about 5e/Å$^3$ at positions corresponding to T* atoms in

mullite (but here with doubled lattice parameter *c*). The deepest trough is observed at the O3 (also designated Oc in the mullite literature) position clearly indicating a preference for the mullite-type model with oxygen vacancies. Consequently, a series of refinements was performed varying the chemical composition towards the composition of mullite. Plotting the residual in Fig. 5 versus the *x*-value in $Al_{8+4x}Si_{4-4x}O_{20-2x}$ yielded a composition from crystal-structure refinement with $x = 0.12$ corresponding to $Al_{8.48}Si_{3.52}O_{19.76}$. Final refinements with mixed occupancies of Al and Fe on the octahedral and the T*2 position and all atoms but O41 and O42 with anisotropic displacement parameters converged at R1 = 5.9%. Residual electron density of about 1 e/Å$^3$ shows that the crystal structure is essentially correct but might indicate that split positions could be possible due to the local distortions around the oxygen vacancies. Final atomic parameters are listed in Table 3 and selected interatomic distances in Table 4.

## Discussion

**General description.** The chemical composition of the new phase „sillimullite“ derived from electron microprobe analyses is very close to that of sillimanite (Table 2). Contrary to this, the $Al_2O_3$ composition calculated from crystal structure refinement on the basis of the single-crystal diffraction data (Table 1) is significantly higher. The discrepancy between both data sets is shown in Fig. 3 where the lattice parameters are plotted versus the $Al_2O_3$ content. Lattice parameter *a* plotted for the composition determined from the crystal-structure refinement (green cross) follows closely the linear trend observed for mullites while the corresponding parameter for the microprobe results (red cross) is clearly off this trend.

Similarly, plotting the lattice parameters versus $Fe_2O_3$ mole fractions in Fig. 4 shows that “sillimullite” is distinctly different from sillimanite. The data points of “sillimullite” are compared with those of iron bearing sillimanites taken from Table 6 in Grew (1980). While *b* follows the linear trend pretty well, *a* and *c* are significantly higher than the corresponding values for the sillimanites.

The results of the crystal-structure refinement revealed that the mineral species studied here, designated as „sillimullite“, neither corresponds to sillimanite nor to mullite. On the one hand, it has an ordering scheme with a Si/Al distribution similar to sillimanite causing the doubling of *c* with respect to that of mullite. On the other hand, it has the oxygen vacancies coupled with the formation of triclusters typical for mullite. The distribution of Si and Al is strictly alternating in an individual *zweier* double chain of $TO_4$ (T = Al,Si) tetrahedra but it is shifted by ½ of a unit cell in **c** for neighboring chains as compared with sillimanite shown in Fig. 6a. For an easier comparison, oxygen vacancies and triclusters are omitted in the structure projections of „sillimullite“ in Fig. 6. Fig. 6c shows the crystal structure transformed to the *Pbnm* setting by interchanging **a** and **b** axes representing the space-group setting of sillimanite but having another orientation of the octahedral and tetrahedral chains as compared with sillimanite or mullite. The octahedral axis in the **ab**-plane is closer to **b**-axis in the *Pnam* setting shown in Fig. 6b in agreement with the orientation of the octahedra in sillimanite (Fig. 6a) and the description of mullite and mullite-type compounds with symmetries lower than tetragonal (Fischer and Schneider 2005; Fischer and Schneider 2008; Fischer et al. 2012). Fig. 7 shows the crystal structure including oxygen vacancy and tricluster formation.

The biggest puzzle in this investigation was the evaluation of the chemical composition of „sillimullite“ as determined from microprobe analyses and from crystal structure refinements. The chemical composition was checked carefully on two different electron microprobes and yielded $Al_2O_3$ contents close to that of sillimanite. The diffraction-derived chemical composition deviated from the microprobe data in showing significantly higher $Al_2O_3$ contents than in sillimanite, and there was no doubt from the refinements that the crystal contains oxygen vacancies accompanied by tricluster formation. At present, the most probable explanation of the discrepant data would be a segregation process of amorphous nanosized

$SiO_2$ particles in an aluminosilicate matrix being slightly enriched in $Al_2O_3$ with respect to sillimanite. Such amorphous nanosized $SiO_2$ particles would be detected by the microprobe but they would not affect the diffraction intensities. Comparable $SiO_2$ exsolution from a sillimanite matrix were described by Holland and Carpenter (1986) investigating the behavior of sillimanite at high pressure and temperature by transmission electron microscopy (TEM). Holland and Carpenter (1986) mentioned that sillimanite at $p \approx 1.8$-2 GPa and T ≈ 1300 to 1700°C transforms to a gradually disordered sillimanite enriched in $Al_2O_3$ (up to $x \approx 0.1$), accompanied by a $SiO_2$-rich glass phase (< 0.1 μm). Rahman et al. (2001) described the complete transformation of sillimanite to 3/2-mullite with precipitations of amorphous $SiO_2$ upon thermal treatment at 1600°C for 24 hs. Here the $SiO_2$ is formed in nanosized channels parallel to the **c**-axis of the former sillimanite (Schneider and Schmücker 2005). If the reaction had not gone to completion, coexisting sillimanite and mullite are found and exsolved $SiO_2$ might be present in the sillimanite cavities or on its surface. Guse et al. (1979) pointed out that silica does not crystallize in the mullitization process at 1600°C being present in glassy form. Annealing of an Fe-bearing sillimanite at 1675°C and 2 GPa for 12 min yielded a partial transformation to mullite accompanied by partial melting. The small exsolved precipitates (< 100 nm) were rich in $SiO_2$ (80 wt %) as determined by analytical transmission electron microscopy (ATEM). The exsolution of $SiO_2$ according to $3Al_2SiO_5 \rightarrow$ 3/2-mullite + $SiO_2$ is also the common reaction during the high-temperature induced transformation of the mullite-type aluminosilicate andalusite (Hülsmans et al. 2000a,b). Taking into account that just one $SiO_2$ formula unit is exsolved from the crystal structure of the mineral studied here in every 2nd to 3rd unit cell this might not be detected by analytical methods, especially if the $SiO_2$ remains in cavities of the crystal as observed, e.g. in the exsolution process mentioned above for andalusite. A sillimanite-type superstructure with its ordering of Si and Al essentially is retained and the exsolution does not significantly affect the

crystal-structure refinement. However, the ordering scheme must have changed in this process yielding the ordering pattern of „sillimullite“ (Fig. 8b) which is different from the ordering in sillimanite (Fig. 8a) in the unit-cell settings corresponding to $a < b$.

The fact that exsolution processes in sillimanites have been observed does not mean that the natural “sillimullite” described here underwent the same conditions as in the experimental procedures described above. It just means that such exsolution processes are commonly observed in sillimanite and thus could be basically considered as possible explanation for the discrepancy in the chemical composition of “sillimullite”.

**Si/Al ordering**. The crystal-structure refinement clearly yielded an ordering of Si and Al in the tetrahedral double chains. Compared with literature data listed in Table 5 the mean Si-O distances are slightly larger and the mean Al-O distances are slightly smaller than observed in the sillimanite structures senso stricto. This might indicate that the ordering in „sillimullite“ is not complete similar to that in fibrous sillimanite having about 10% mixed occupancies in the T sites (Bish and Burnham 1992). However, the exact determination of the Si/Al distribution is difficult due to the similarities in the scattering power of Si and Al in the X-ray case. Refinement of simultaneous occupancy of Al and Si on the T(Al) position (Table 3) was not stable. So we performed a series of fixed occupancies similarly to the graph shown in Fig. 5 immediately resulting in a linear increase of R1 when Si was incorporated on this position. Thus, a complete ordering was applied in the refinements.

The main difference in the Si/Al distribution between sillimanite and „sillimullite“ is in the occupancies of neighboring double chains of $TO_4$ tetrahedra as shown in Figs. 6 and 8 causing the different settings of the space-group symmetries. Dislocations with shifts of the chains one half parallel **c** as Burgers vector produce similar effects and were described by Doukhan and Christie (1982), Doukhan et al. (1985), Holland and Carpenter(1986), Lefebvre and

Paquet (1983), Menard and Doukhan(1978), and Wenk(1983), and discussed by Salje (1986). Stacking faults, thus, are commonly observed in sillimanites and lead to Al-Al and Si-Si contacts in the tetrahedral double chains as described by Lefebvre and Paquet(1983). Wenk (1983) described a mullite-sillimanite intergrowth with submicroscopic mullite having doubled lattice parameters *a* and *c* with antiphase boundary structures for both sillimanite and mullite. However, these macroscopic or phase-boundary effects are clearly different from the ordered configuration observed here. Within the double chains the $SiO_4$ and $AlO_4$ tetrahedra are clearly ordered but neighboring double chains are dislocated by ½ in **c** with full translational symmetry of either *Pbmn* (sillimanite) or *Pnam* („sillimullite“).

**Foreign cations.** Microprobe analyses of „sillimullite“ yielded $Fe_2O_3$ contents ranging from 1.95 wt.% to 2.55 wt.%, MgO ≈ 0.20 wt.%, and $TiO_2$ ≈ 0.35 wt.%, Table 2. The crystal-structure refinement yielded a preference for iron in the $AlO_6$ octahedron with 0.17(2) Fe and in the T*2 position with 0.032(16) Fe atoms per unit cell. The minor amounts of Ti and Mg cannot be distinguished from Al and Fe in the refinement. The statement that most of the Fe occurs in the $AlO_6$ octahedron with minor amounts in the T* position is in agreement with other studies on the distribution of $Fe^{3+}$ in sillimanite and mullite. Peterson and McMullan(1986) observed Fe in both octahedral and tetrahedral sites in their neutron diffraction studies of sillimanite. Similar results were obtained by Fisher et al.(1979) from the evaluation of intensities from powder-diffraction experiments of mullite. Mössbauer spectroscopy (Parmentier et al. 1999) revealed three different $Fe^{3+}$ sites in mullite. This was confirmed by Rietveld refinements yielding Fe distributed between octahedral and tetrahedral positions. Soro et al.(2003) observed a preference for $Fe^{3+}$ in the octahedron of mullite formed from kaolins. Hålenius(1979) determined $Fe^{3+}$ and $Fe^{2+}$ just in the octahedral position in sillimanite, but the presence of tetrahedrally coordinated Fe was not generally excluded.

306 According to Mack et al.(2005) using high temperature Mössbauer spectroscopy, $Fe^{3+}$ occurs
307 in mullite at two octahedral sites, one being slightly more distorted than the other, while
308 tetrahedral $Fe^{3+}$ is of minor importance. Rossman et al. (1982) showed that the yellow color
309 in sillimanite is mainly caused by $Fe^{3+}$ in the tetrahedral sites.
310 All these results on sillimanite and mullite support our findings that in „sillimullite“ most of
311 the $Fe^{3+}$ enters the $AlO_6$ octahedron and minor amounts are found in the T* position yielding
312 a slightly colored crystal.
313 The minor amounts of $Mg^{2+}$ and $Ti^{4+}$ cannot be distinguished from Al and $Fe^{3+}$ in the
314 refinement. They occur in approximately equal quantities (0.4 mol% $TiO_2$ and MgO,
315 respectively) and thus together have a 3-valence charge. For simplicity, they have been
316 assigned to the Al and Fe part in the chemical composition but there are no clues on the exact
317 position of these atoms in the crystal structure.
318
319 **Symmetry relationships**. Sillimanite and mullite belong to the family of mullite-type crystal
320 structures as defined by Fischer and Schneider (2005) and Fischer et al. (2012) with the
321 characteristic chains of edge-sharing $AlO_6$ octahedra. The new mineral „sillimullite“
322 intermediate between sillimanite and mullite conforms to the criteria listed in these references.
323 However, it represents a new branch in the symmetry relationships derived from the
324 hypothetical tetragonal aristotype. Fig. 9 shows the symmetry relationships in the
325 Bärnighausen tree (Bärnighausen 1980) of group-subgroup representations. The new mineral
326 has a symmetry representing a subgroup of mullite similar with sillimanite and andalusite in
327 *klassengleiche* subgroups of index 2. Mullite is assigned to group 3 in the Bärnighausen tree
328 of the mullite family (Fischer and Schneider 2005), andalusite represents the first and
329 sillimanite the second derivative, thus having numbers 31 (branch 3 position 1) and 32
330 (branch 3 position 2), respectively. The new mineral is assigned to position 6 because 3 is

already assigned to $Al_{18}B_4O_{33}$, 4 to mozartite, and 5 to boralsilite and werdingite (see Fischer and Schneider 2005; Fischer et al. 2012).

## Implications

„Sillimullite“, a new mineral studied here, has characteristic features of both sillimanite (Si/Al ordering, doubled *c* lattice parameter) and mullite (oxygen vacancies, formation of triclusters) but it is distinctly different from both minerals. In this respect, it is expanding the current knowledge on sillimanite and mullite type compounds. As a rare mineral it might be just a curiosity, but it implies that compounds similar but significantly different to mullite do exist and might represent new members of the mullite family. Compared to sillimanite, the tetrahedral double chains are shifted ½ parallel **c** yielding a different sequence of $AlO_4$ and $SiO_4$ tetrahedra in the (001) plane with the effect that the space group symmetry changes to *Pnam* which is a different setting of the sillimanite space group *Pbnm*. Therefore, „sillimullite“ could be considered to represent a new mineral intermediate between sillimanite and mullite.

## Acknowledgement

We gratefully acknowledge the support of the Deutsche Forschungsgemeinschaft funding this work under grant Fi442/17-1. We thank Martin Erdmann and Anika Husen for their support at the microprobe at the Institut für Mineralogie, Leibniz Universität Hannover, Angelika Freesemann for preparing the polished crystal for the microprobe analyses, Ed Grew and Ronald Miletich for their comments which substantially improved the quality of this manuscript, and Michael Wendschuh and Hanna Lührs for their assistance in drawing Fig. 4.

## References

Bärnighausen, H. (1980) Group-subgroup relations between space groups: A useful tool in crystal chemistry. Communications in mathematical chemistry MATCH, 9, 209-233.

Bish, D.L., and Burnham, C.W. (1992) Rietveld refinement of the crystal structure of fibrolitic sillimanite using neutron powder diffraction data. American Mineralogist, 77, 374-379.

Blaß, G., and Graf, H.W. (1994) Über neue Mineralien vom Bellerberg, Eifel. Mineralien-Welt 05/6, 53-56.

Burnham, C.W. (1963) Refinement of the crystal structure of sillimanite. Zeitschrift für Kristallographie, 118, 127-148.

Burnham, C.W. (1964) The crystal structure of mullite. Carnegie Institution of Washington Year Book, 62, 158-165.

Cameron, W.E. (1976a) Coexisting sillimanite and mullite. Geological Magazine, 113, 497-515.

Cameron, W.E. (1976b) A mineral phase intermediate in composition between sillimanite and mullite. American Mineralogist, 61, 1025-1026.

Cameron, W.E. (1977) Nonstoichiometry in sillimanite: Mullite compositions with sillimanite-type superstructures. Physics and Chemistry of Minerals, 1, 265-272.

Doukhan, J.C., and Christie, J.M. (1982) Plastic deformation of sillimanite $Al_2SiO_5$ single crystals under confining pressure and TEM investigation of the induced defect structure. Bulletin de Minéralogie, 105, 583-589.

Doukhan, J.C., Doukhan, N., Koch, P.S., and Christie, J.M. (1985) Transmission electron microscopy investigation of lattice defects in $Al_2SiO_5$ polymorphs and plasticity induced polymorphic transformations. Bulletin de Minéralogie, 108, 81-96.

Ďurovič, S. (1962) Isomorphism between sillimanite and mullite. Journal of the American Ceramic Society, 45, 157-161.

Ďurovič, S., and Dávidová, Š. (1962) Refined atomic coordinates for sillimanite structure. Acta Crystallographica, 15, 1051.

Dzikowski, T.J., Groat, L.A., Grew, E.S. (2007) The geometric effects of $^{V}Fe^{2+}$ for $^{V}Mg$ substitution on the crystal structures of the grandidierite-ominelite series. American Mineralogist, 92, 863-872.

Ebadzadeh, T. and Sharifi, L. (2008) Synthesis of ι- $Al_2O_3$ from a mixture of aluminum nitrate and carboxylmethyl cellulose. J. Amer. Ceram. Soc. 91, 3408-3409,

Farrugia, L.J. (1999) WinGX suite for small-molecule single-crystal crystallography. Journal of Applied Crystallography, 32, 837-838.

Fischer, R.X., and Messner, T. (2013) STRUPLO, a new version of the structure drawing program. Fachbereich Geowissenschaften, Universität Bremen.

Fischer, R.X., and Schneider, H. (2005) The mullite-type family of crystal structures. In H. Schneider, and S. Komarneni, Eds. Mullite, p. 1-46. Wiley-VCH, Weinheim.

Fischer, R.X., and Schneider, H. (2008) Crystal chemistry of borates and borosilicates with mullite-type structures: a review. European Journal of Mineralogy, 20, 917-933.

Fischer, R.X., Gaede-Köhler, A., Birkenstock, J., and Schneider, H. (2012) Mullite and mullite-type crystal structures. International Journal of Materials Research, 103, 402-407.

Fisher, O.N., Smyslov, Y.N., and Shmitt-Fogelevich, S.P. (1979) Determination of the structural position of Fe3+ in mullite by powder diffractometry. Journal of Structural Chemistry, 20, 926-930.

Grew, E.S. (1980) Sillimanite and ilmenite from high-grade metamorphic rocks of Antarctica and other areas. Journal of Petrology, 21, 39-68.

Grew, E.S., Hinthorne, J.R. (1983) Boron in sillimanite. Science, 221, 547-549.

Grew, E.S., Rossman, G.R. (1985) Co-ordination of boron in silimanite. Mineralogical Magazine, 49, 132-135.

Guse, W., Saalfeld, H., and Tjandra, J. (1979) Thermal transformation of sillimanite single crystals. Neues Jahrbuch für Mineralogie Monatshefte, 175-181.

Hahn, T. (2005) International Tables for Crystallography. Springer.

Hålenius, U. (1979) State and location of iron in sillimanite. Neues Jahrbuch Mineralogie Monatshefte, 165-174.

Hariya, Y., Dollase, W.A., and Kennedy, G.C. (1969) An experimental investigation of the relationship of mullite to sillimanite. American Mineralogist, 54, 1419-1441.

Holland, T.J.B., and Carpenter, M.A. (1986) Aluminium/silicon disordering and melting in sillimanite at high pressures. Nature, 320, 151-153.

Hülsmans, A., Schmücker, M., Mader, W., and Schneider, H. (2000a) The transformation of andalusite to mullite and silica: Part I. Transformation mechanism in $[001]_A$ direction. American Mineralogist, 85, 980-986.

Hülsmans, A., Schmücker, M., Mader, W., and Schneider, H. (2000b) The transformation of andalusite to mullite and silica: Part II. Transformation mechanisms in $[100]_A$ and $[010]_A$ directions. American Mineralogist, 85, 987-992.

Lefebvre, A., and Paquet, J. (1983) Dissociation of *c* dislocations in sillimanite $Al_2SiO_5$. Bulletin de Minéralogie, 106, 287-292.

Mack, D.E., Becker, K.D., and Schneider, H. (2005) High-temperature Mössbauer study of Fe-substituted mullite. American Mineralogist, 90, 1078-1083.

Menard, D., and Doukhan, J.C. (1978) Défauts de réseau dans la sillimanite: $Al_2O_3$-$SiO_2$. Journal de Physique Lettres, 39, L19-L22.

Parmentier, J., Vilminot, S., and Dormann, J.L. (1999) Fe- and Cr-substituted mullites: Mössbauer spectroscopy and Rietveld structure refinement. Solid State Sciences, 1, 257-265.

Perrotta, A.J., and Young, J.E. (1974) Silica-free phases with mullite-type structures. Journal of the American Ceramic Society, 57, 405-407.

Peterson, R.C., and McMullan, R.K. (1986) Neutron diffraction studies of sillimanite. American Mineralogist, 71, 742-745.

Petříček, V., Dušek, M., and Palatinus, L. (2006) Jana2006. The crystallographic computing system. , Institute of Physics, Praha, Czech Republic.

Pouchou, J.L., and Pichoir, F. (1991) Quantitative analysis of homogeneous or stratified microvolumes applying the model ‘‘PAP’’. In K.F.J. Heinrich, and D.E. Newbury, Eds. Electron Probe Quantitation, p. 31-75.

Rahman, S., Feustel, U., and Freimann, S. (2001) Structure description of the thermic phase transformation sillimanite-mullite. Journal of the European Ceramic Society, 21, 2471-2478.

Raterron, P., Carpenter, M., Doukhan, J.C. (1999) Sillimanite mullitization: ATEM investigation and point defect model. Phase Transitions, 68, 481-500.

Rossman, G.R., Grew, E.S., and Dollase, W.A. (1982) The colors of sillimanite. American Mineralogist, 67, 749-761.

Salje, E. (1986) Heat capacities and entropies of andalusite and sillimanite: The influence of fibrolitization on the phase diagram of the $Al_2SiO_5$ polymorphs. American Mineralogist, 71, 1366-1371.

Schneider, H., Fischer, R.X., and Voll, D. (1993) Mullite with lattice constants a > b. Journal of the American Ceramic Society, 76, 1879-1881.

Schneider, H., and Schmücker, M. (2005) Structure-controlled formation and decomposition of mullite. In H. Schneider, and S. Komarneni, Eds. Mullite, p. 167-180. Wiley-VCH, Weinheim.

Sheldrick, G.M. (1997) SHELXL-97, a program for crystal structure refinement. University of Goettingen.

Sheldrick, G.M. (2008) A short history of SHELX. Acta Crystallographica A64, 112-122.

Soro, N., Aldon, L., Olivier-Fourcade, J., Jumas, J.C., Laval, J.P., and Blanchart, P. (2003) Role of iron in mullite formation from kaolins by Mössbauer spectroscopy and Rietveld refinement. Journal of the American Ceramic Society, 86, 129-134.

Taylor, W.H. (1928) The structure of sillimanite and mullite. Zeitschrift für Kristallographie, 68, 503-521.

Wenk, H.R. (1983) Mullite-sillimanite intergrowth from pelitic inclusions in Bergell tonalite. Neues Jahrbuch für Mineralogie Abhandlungen, 146, 1-14.

Winter, J.K., and Ghose, S. (1979) Thermal expansion and high-temperature crystal chemistry of the $Al_2SiO_5$ polymorphs. American Mineralogist, 64, 573-586.

Yang, H., Hazen, R.M., Finger, L.W., Prewitt, C.T., and Downs, R.T. (1997) Compressibility and crystal structure of sillimanite, $Al_2SiO_5$, at high pressure. Physics and Chemistry of Minerals, 25, 39-47.

List of figure captions

Fig. 1: Microprobe images of „sillimullite“ obtained on two different instruments with instrumental parameters listed in Table 2. a) Leibniz Universität Hannover. b) TU Clausthal

Fig. 2: 0kl layer of the „sillimullite“ crystal calculated from all 2D frames of the full data set. View parallel to **a*, c*** pointing down, **b*** pointing right. Inset in the upper right with enlarged central area: The smaller grey frame refers to the „sillimullite“ reciprocal unit cell, the larger white one to mullite, indicating the doubling of **c** in „sillimullite“.

Fig. 3: Lattice parameters of the $Al_{4+2x}Si_{2-2x}O_{10-x}$ aluminosilicate solid solution series with mullite-type structures from sillimanite (50 mol% $Al_2O_3$) and hypothetical ι-alumina (100 mol% $Al_2O_3$). The *a* and *b* parameters are scaled to the left ordinate, *c* to the right one being halved for sillimanite and „sillimullite“ for comparison with mullite. Red crosses indicate compositions derived from microprobe analyses, green crosses refer to the results of the structure refinement with Fe assigned to Al. Black crosses represent average values for sillimanite calculated from the five entries in Table 5. Modified from Fig. 1.1.13 of Fischer and Schneider (2005) to include data on sillimanite and “sillimullite”.

Fig. 4: Lattice parameters plotted versus molar fractions of $Fe_2O_3$ in “sillimullite” (diamond symbol) in comparison to those of iron-bearing sillilmanites (crosses) given by Grew (1980).

Fig. 5: Residual R1 plotted vs. *x*-value in $Al_{8+4x}Si_{4-4x}O_{20-2x}$.

Fig. 6: Crystal structure projections of sillimanite and „sillimullite“ in the two space-group settings in an idealized representation ignoring oxygen vacancies and triclusters in „sillimullite“. Identical sequences of Si and Al in the tetrahedral double chains are encircled

by a green oval and different sequences by a red oval. Neighboring double chains are shifted by ½ unit cell parallel to **c**. Blue polyhedra are occupied by Al, yellow ones by Si. View parallel to **c** rotated by 6° about **a** and **b**.

a) Sillimanite in space group *Pbnm* (Yang et al. 1997). b) The crystal structure of „sillimullite“ in *Pnam*. c) The crystal structure of „sillimullite“ transformed to *Pbnm* setting according to **b**, **a**, **-c**.

Fig. 7: Crystal-structure projection of „sillimullite“ with an oxygen vacancy in 1, ½, 1. Triclusters consisting of two $TO_4$ and one $T^*O_4$ groups are dark blue. The colors of the other polyhedra correspond to those in Fig.6. O atoms are omitted for clarity. View parallel **c** rotated by 4° about **a** and **b**. a) Representation of four unit cells. One is outlined in the upper left part. b) The upper layer with one oxygen vacancy.

Fig. 8: Crystal structure projections of the tetrahedral double chains in sillimanite and „sillimullite“. The right double chains correspond to the encircled chains in Fig. 6, the left double chains correspond to the chains in ½,0,*z* in Figs. 6a and b. Colors are assigned as in Fig. 6. View parallel a rotated by 20° about **c** and 5° about **b**. a) sillimanite. b) „sillimullite“.

Fig. 9: The Bärnighausen tree illustrating the symmetry relationships of „sillimullite“ in comparison to those of mullite, sillimanite and andalusite. The branches are derived from a hypothetical aristotype representing the highest possible symmetry. Letters *t* and *k* represent the type of symmetry reduction (*t* = translationengleich, *k* = klassengleich), followed by the index (factor) of symmetry reduction and the origin shift in parentheses. Underneath, the set of basis vectors is given which describes the transformation of a unit cell to its setting in the

subgroup. Space groups representing observed crystal structures are put in frames. Numbers in parentheses behind the space-group symbol refer to the space-group number in the International Tables for Crystallography (Hahn 2005). Roman numerals refer to the index of symmetry reduction relative to the aristotype. Members on one level are distinguished by Arabic numerals carrying the root numbers of the supergroup.

546

547 Table 1: Data collection parameters, refinement details, and crystal data

| | |
|---|---|
| **Crystal data** | |
| Chemical composition from microprobe analyses | $Al_{7.84}Fe_{0.18}Ti_{0.03}Mg_{0.03}Si_{3.92}O_{19.96}$, $x = 0.02$[a] |
| Chemical composition from crystal-structure analysis | $Al_{8.28}Fe_{0.20}Si_{3.52}O_{19.76}$, $x = 0.12$[a] |
| Space group | *Pnam* |
| $Z$ | 1 |
| $a$ (Å) | 7.5127(4) |
| $b$ (Å) | 7.6823(4) |
| $c$ (Å) | 5.7849(7) |
| $V$ (Å$^3$) | 333.87(4) |
| **Data collection and refinement** | |
| Temperature (K) | 298 |
| no. of measured reflections | 24067 |
| no. of unique reflections | 1577 |
| no. $F_o > 4\sigma(F_o)$ | 1024 |
| range of $h$, $k$, $l$ | $\lvert h \rvert \leq 15, \lvert k \rvert \leq 15, \lvert l \rvert \leq 11$ |
| θ-max (°) | 46.53 |
| no. parameters | 70 |
| no. constraints | 0 |
| $R_{int}$ / $R_\sigma$ [b] | 0.0797 / 0.0308 |
| $R1$ / $R1 > 4\sigma(F_o)$ [b] | 0.092 / 0.059 |

| | |
|---|---|
| w$R2$ [b] | 0.1234 |
| GoF [b] | 1.139 |
| min Δ (eÅ$^{-3}$) | -1.14, 0.34 Å from T(Al) |
| max Δ (eÅ$^{-3}$) | 0.96, 0.56 Å from O11 |

[a] $x$ refers to the solid-solution series $Al_{4+2x}Si_{2-2x}O_{10-x}$ (or $Al_{8+4x}Si_{4-4x}O_{20-2x}$)assigning Fe, Ti, and Mg to the Al site. It represents the number of oxygen vacancies in the unit cell of mullite with **c**(mullite) = ½ **c**(„sillimullite“).

[b] $R_{int} = \frac{\sum|F_o^2 - F_o^2(mean)|}{\sum F_o^2}$, $R_\sigma = \frac{\sum \sigma(F_o^2)}{\sum F_o^2}$, $R1 = \frac{\sum||F_o|-|F_c||}{\sum|F_o|}$, $wR2 = \left(\frac{\sum w(F_o^2 - F_c^2)^2}{\sum w(F_o^2)^2}\right)$, $w = \frac{1}{\left(\sigma(F_o^2)\right)^2 + (0.0278 \cdot P)^2 + 1.35 \cdot P}$, $P = \frac{max(F_o^2, 0) + 2 \cdot F_c^2}{3}$, $GoF = \sqrt{\frac{\sum w(F_o^2 - F_c^2)^2}{n-p}}$, n = number of reflections, p = total number of parameters refined.

Table 2: Electron microprobe analyses of “sillimullite”. Results are given in weight percent.

Leibniz Universität Hannover

| spot | $SiO_2$ | $Al_2O_3$ | $Fe_2O_3$ | $TiO_2$ | MgO | total |
|---|---|---|---|---|---|---|
| 1 | 35.02 | 59.65 | 2.11 | 0.33 | 0.22 | 97.32 |
| 2 | 35.34 | 60.47 | 2.13 | 0.44 | 0.22 | 98.59 |
| 7 | 36.60 | 60.62 | 2.32 | 0.27 | 0.23 | 100.04 |

TU Clausthal

| spot | $SiO_2$ | $Al_2O_3$ | $Fe_2O_3$ | $TiO_2$ | MgO | total |
|---|---|---|---|---|---|---|
| 5 | 36.21 | 60.32 | 2.56 | 0.34 | 0.20 | 99.62 |
| 6 | 36.59 | 61.06 | 2.49 | 0.31 | 0.20 | 100.65 |
| 7 | 36.20 | 62.14 | 1.97 | 0.14 | 0.12 | 100.56 |
| 8 | 36.13 | 62.01 | 2.23 | 0.37 | 0.26 | 101.01 |
| 9 | 37.24 | 62.11 | 2.16 | 0.52 | 0.18 | 102.21 |
| 10 | 35.66 | 62.61 | 2.11 | 0.52 | 0.20 | 101.10 |
| 11 | 36.75 | 62.01 | 2.03 | 0.41 | 0.22 | 101.43 |
| 12 | 36.44 | 62.53 | 1.95 | 0.18 | 0.17 | 101.27 |
| 13 | 36.23 | 61.96 | 2.39 | 0.27 | 0.25 | 101.10 |

Average composition derived from all spots (Hannover and Clausthal) listed above scaled to 100 wt% with standard deviations for the last significant digit in parentheses, compared to corresponding compositions of pure sillimanite and 3/2-mullite

| mean over all | $SiO_2$ | $Al_2O_3$ | $Fe_2O_3$ | $TiO_2$ | MgO | total |
|---|---|---|---|---|---|---|
| 12 spots | 36.1(6) | 61.2(1.0) | 2.2(2) | 0.3(1) | 0.21(4) | 100(2) |
| sillimanite | 37.1 | 62.9 | | | | |
| 3/2-mullite | 28.2 | 71.8 | | | | |

Table 2b: Electron microprobe analyses recalculated to atomic composition per unit cell

Leibniz Universität Hannover

| spot | Si | Al | Fe | Ti | Mg | O |
|---|---|---|---|---|---|---|
| 1 | 3.910 | 7.849 | 0.177 | 0.028 | 0.037 | 19.950 |
| 2 | 3.895 | 7.855 | 0.177 | 0.036 | 0.036 | 19.948 |
| 7 | 3.981 | 7.770 | 0.190 | 0.022 | 0.037 | 19.983 |

TU Clausthal

| spot | Si | Al | Fe | Ti | Mg | O |
|---|---|---|---|---|---|---|
| 5 | 3.958 | 7.771 | 0.211 | 0.028 | 0.033 | 19.977 |
| 6 | 3.957 | 7.783 | 0.203 | 0.025 | 0.032 | 19.975 |
| 7 | 3.906 | 7.903 | 0.160 | 0.011 | 0.019 | 19.949 |
| 8 | 3.886 | 7.861 | 0.181 | 0.030 | 0.042 | 19.937 |
| 9 | 3.964 | 7.792 | 0.173 | 0.042 | 0.029 | 19.989 |
| 10 | 3.830 | 7.925 | 0.171 | 0.042 | 0.032 | 19.920 |
| 11 | 3.938 | 7.831 | 0.164 | 0.033 | 0.035 | 19.968 |

| | | | | | | |
|---|---|---|---|---|---|---|
| 12 | 3.905 | 7.897 | 0.157 | 0.015 | 0.027 | 19.946 |
| 13 | 3.895 | 7.850 | 0.193 | 0.022 | 0.040 | 19.938 |

574

575 Average composition per unit cell derived from all spots (Hannover and Clausthal) compared
576 to corresponding compositions of pure sillimanite and 3/2-mullite

| mean over all | Si | Al | Fe | Ti | Mg | O |
|---|---|---|---|---|---|---|
| 12 spots | 3.92(4) | 7.84(5) | 0.180(17) | 0.028(10) | 0.033(6) | 19.96(2) |
| sillimanite | 4 | 8 | | | | |
| 3/2-mullite | 3 | 9 | | | | |

577

578

579

580 **Table 3.** Atomic coordinates, Wyckoff positions, site occupancies (occ.), and anisotropic

581 displacement parameters (Å²).

| atom | Wyck. | *x* | *y* | *z* | occ. | $U_{eq}$ (Å²) |
|---|---|---|---|---|---|---|
| (Al,Fe) | 4a | 0 | 0 | 0 | 0.958/0.042(4) | 0.0056(2) |
| T(Al) | 4c | 0.1488(1) | 0.3400(1) | 0.25 | 1.0 | 0.0080(2) |
| T(Si) | 4c | 0.14668(9) | 0.34296(9) | 0.75 | 0.88 | 0.0036(1) |
| T*1(Al) | 4c | 0.2627(17) | 0.2076(17) | 0.25 | 0.06 | 0.006(2) |
| T*2(Al,Fe) | 4c | 0.259(2) | 0.204(2) | 0.75 | 0.052/0.008(4) | 0.011(3) |
| O11 | 4c | 0.3669(2) | 0.4171(3) | 0.25 | 1.0 | 0.0082(3) |
| O12 | 4c | 0.3490(2) | 0.4261(3) | 0.75 | 1.0 | 0.0089(3) |
| O2 | 8d | 0.1265(2) | 0.2221(2) | -0.0116(2) | 1.0 | 0.0093(2) |
| O3 | 4c | -0.0004(4) | 0.5075(4) | 0.25 | 0.82 | 0.0128(4) |
| O41 | 4c | 0.451(4) | 0.048(5) | 0.25 | 0.06 | 0.008(5)[a] |
| O42 | 4c | 0.450(5) | 0.054(5) | 0.75 | 0.06 | 0.009(5)[a] |

582 [a] isotropic displacement parameters

| Atom | $U_{11}$ | $U_{22}$ | $U_{33}$ | $U_{23}$ | $U_{13}$ | $U_{12}$ |
|---|---|---|---|---|---|---|
| (Al,Fe) | 0.0056(3) | 0.0056(3) | 0.0055(3) | -0.0004(2) | -0.0002(2) | 0.0002(2) |
| T(Al) | 0.0078(3) | 0.0083(3) | 0.0078(3) | 0 | 0 | 0.0000(2) |
| T(Si) | 0.0029(2) | 0.0043(3) | 0.0036(3) | 0 | 0 | -0.0007(2) |
| T*1(Al) | 0.005(4) | 0.007(4) | 0.005(4) | 0 | 0 | 0.001(4) |
| T*2(Al,Fe) | 0.012(6) | 0.013(5) | 0.009(5) | 0 | 0 | -0.003(4) |
| O11 | 0.0068(6) | 0.0114(7) | 0.0065(6) | 0 | 0 | -0.0032(5) |
| O12 | 0.0066(6) | 0.0122(7) | 0.0080(6) | 0 | 0 | -0.0040(6) |
| O2 | 0.0097(4) | 0.0083(4) | 0.0098(4) | -0.0005(4) | 0.0007(4) | -0.0030(3) |
| O3 | 0.0140(9) | 0.0109(9) | 0.0134(9) | 0 | 0 | 0.0062(8) |

583

584

585 Table 4: Selected interatomic distances (Å).

| octahedron | | $T(Al)-O_4$ | | $T(Si)-O_4$ | |
|---|---|---|---|---|---|
| 2×(Al,Fe)-O11 | 1.870(1) | Al-O3 | 1.707(4) | Si-O3 | 1.590(4) |
| 2×(Al,Fe)-O12 | 1.924(1) | Al-O11 | 1.742(2) | Si-O12 | 1.649(2) |
| 2×(Al,Fe)-O2 | 1.954(1) | 2×Al-O2 | 1.772(1) | 2×Si-O2 | 1.670(1) |
| mean | 1.916 | mean | 1.748 | mean | 1.645 |

| $T1*(Al)-O_{4+1}$ | | $T2*(Al,Fe)-O_{4+1}$ | |
|---|---|---|---|
| Al-O11 | 1.79(1) | 2× (Al,Fe)-O2 | 1.709(8) |
| 2×Al-O2 | 1.830(7) | (Al,Fe)-O42 | 1.82(4) |
| Al-O41 | 1.87(3) | (Al,Fe)-O12 | 1.84(1) |
| Al-O12 | 2.32(1) | (Al,Fe)-O11 | 2.40(1) |
| mean 4 | 1.83 | mean 4 | 1.77 |
| mean 5 | 1.93 | mean 5 | 1.90 |

586

587

588 Table 5: Mean M-O distances (Å) in tetrahedral and octahedral coordinations in sillimanites
589 and in „sillimullite“.

590

| Al in octahedron | Al in tetrahedron | Si in tetrahedron | method[b] | reference[c] |
|---|---|---|---|---|
| space group *Pbnm* | | | | |
| 1.912(3) | 1.770(5) | 1.614(5) | SX | Burnham(1963) |
| 1.912(1) | 1.763(3) | 1.627(3) | SX | Winter and Ghose (1979) |
| 1.912(5) | 1.759(1) | 1.623(1) | PN | Peterson and McMullan (1986) |
| 1.912(1) | 1.754(2)[a] | 1.633(2)[a] | PX | Bish and Burnham (1992) |
| 1.913(1) | 1.762(2) | 1.623(2) | SX | Yang et al. (1997) |
| 1.912 | 1.762 | 1.624 | mean[d] | |
| space group *Pnam* | | | | |
| 1.916(1) | 1.748(2) | 1.645(2) | SX | this work |

591 [a] mixed occupancies with about 10% Si in the Al site and 10% Al in the Si site.

592 [b] S refers to single-crystal diffraction, P to powder diffraction, X to X-ray, and N to neutron
593 radiation.

594 [c] The results of the refinements by Taylor (1928) and Ďurovič and Dávidová (1962) are
595 omitted here because of low quality and missing lattice parameters, respectively.

596 [d] Mean values are calculated from the five sillimanite entries.

597

598

599

600

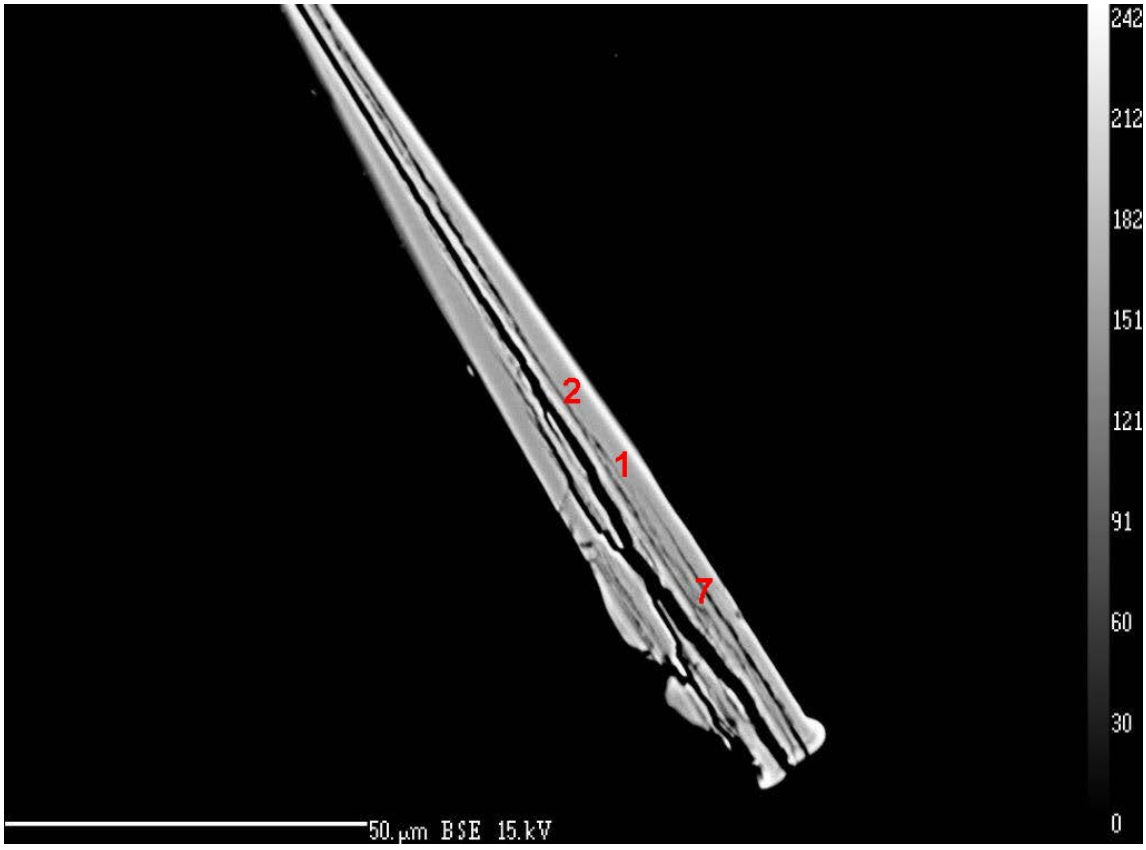


601

602 a) Leibniz Universität Hannover.

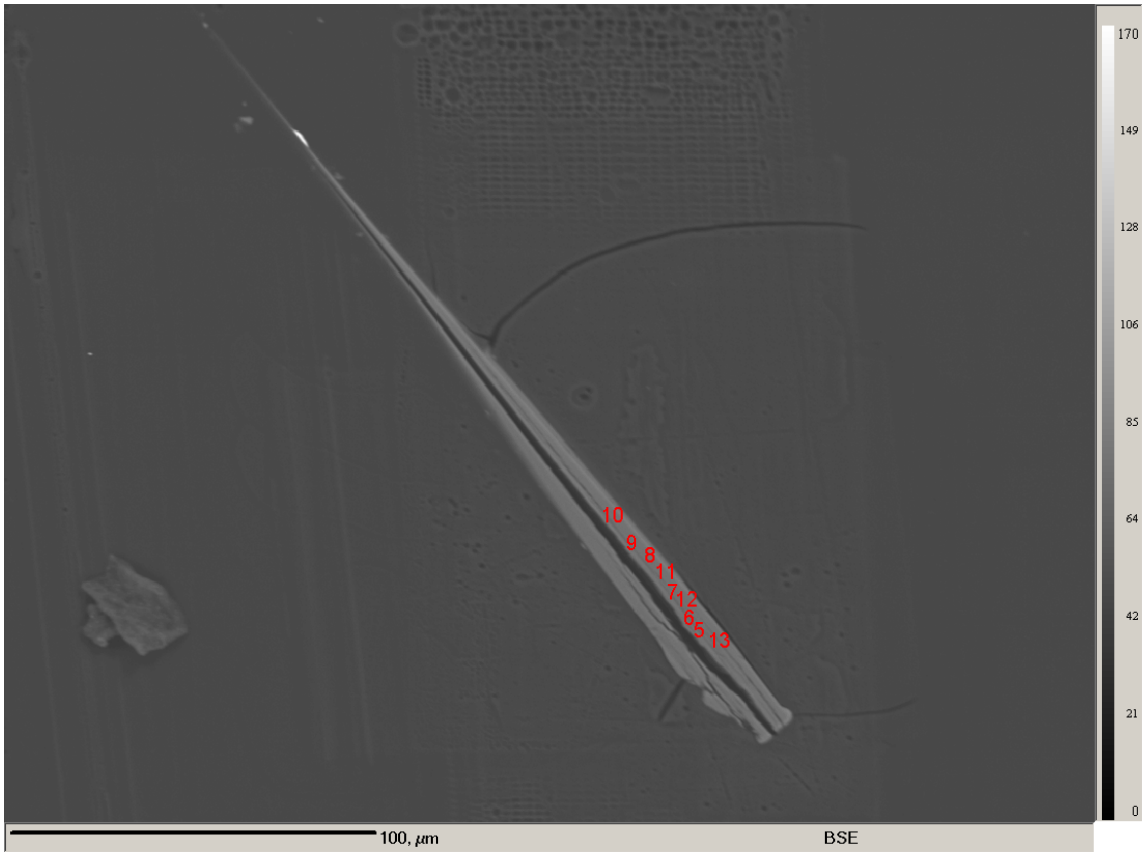


b) TU Clausthal

Fig. 1: Microprobe images of „sillimullite“ obtained on two different instruments with instrumental parameters listed in Table 2.

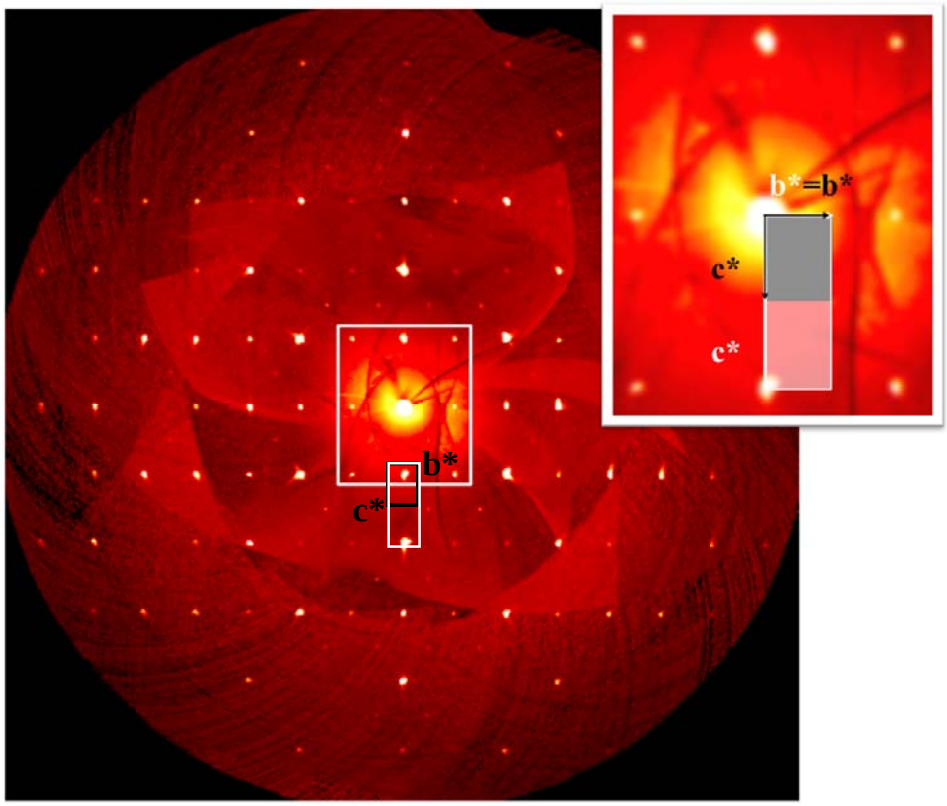


608

609 Fig. 2: 0kl layer of the „sillimullite“ crystal calculated from all 2D frames of the full data set.

610 View parallel to **a*, c*** pointing down, **b*** pointing right. Inset in the upper right with enlarged

611 central area: The smaller grey frame refers to the „sillimullite“ reciprocal unit cell, the larger

612 white one to mullite, indicating the doubling of **c** in „sillimullite“.

613

614

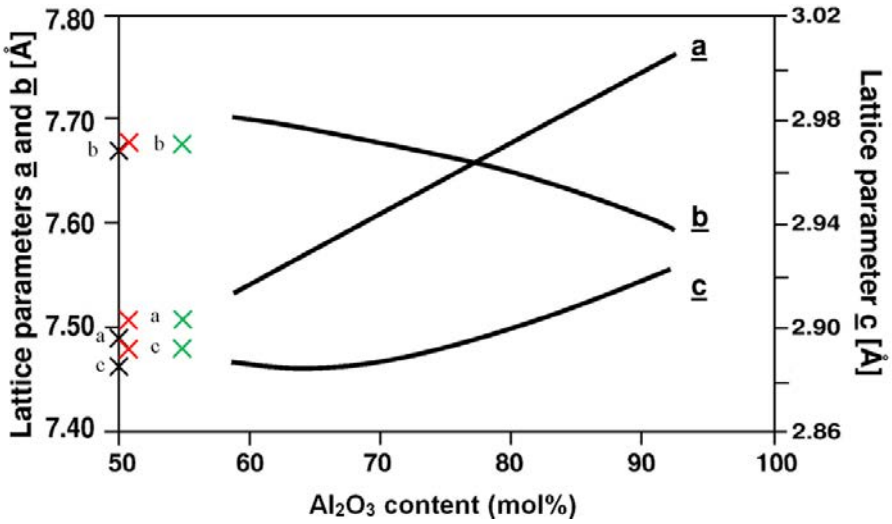


615

616

617 Fig. 3: Lattice parameters of the $Al_{4+2x}Si_{2-2x}O_{10-x}$ aluminosilicate solid solution series with
618 mullite-type structures from sillimanite (50 mol% $Al_2O_3$) and hypothetical ι-alumina (100
619 mol% $Al_2O_3$). The *a* and *b* parameters are scaled to the left ordinate, *c* to the right one being
620 halved for sillimanite and „sillimullite“ for comparison with mullite. Red crosses indicate
621 compositions derived from microprobe analyses, green crosses refer to the results of the
622 structure refinement with Fe assigned to Al. Black crosses represent average values for
623 sillimanite calculated from the five entries in Table 5. Modified from Fig. 1.1.13 of Fischer
624 and Schneider (2005) to include data on sillimanite and “sillimullite”.

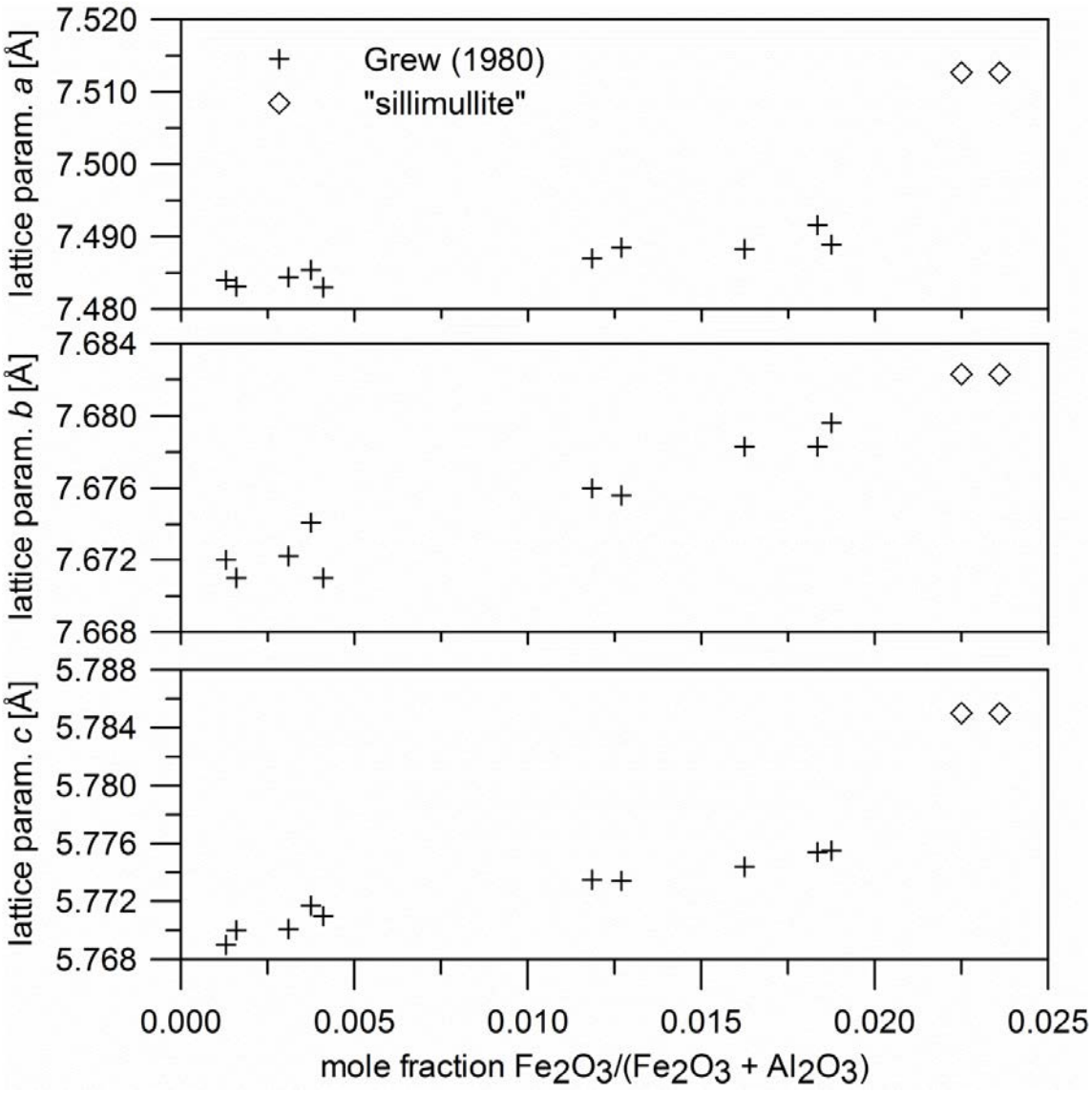


Fig. 4: Lattice parameters plotted versus molar fractions of $Fe_2O_3$ in “sillimullite” (diamond symbol) in comparison to those of iron-bearing sillilmanites (crosses) given by Grew (1980).

634

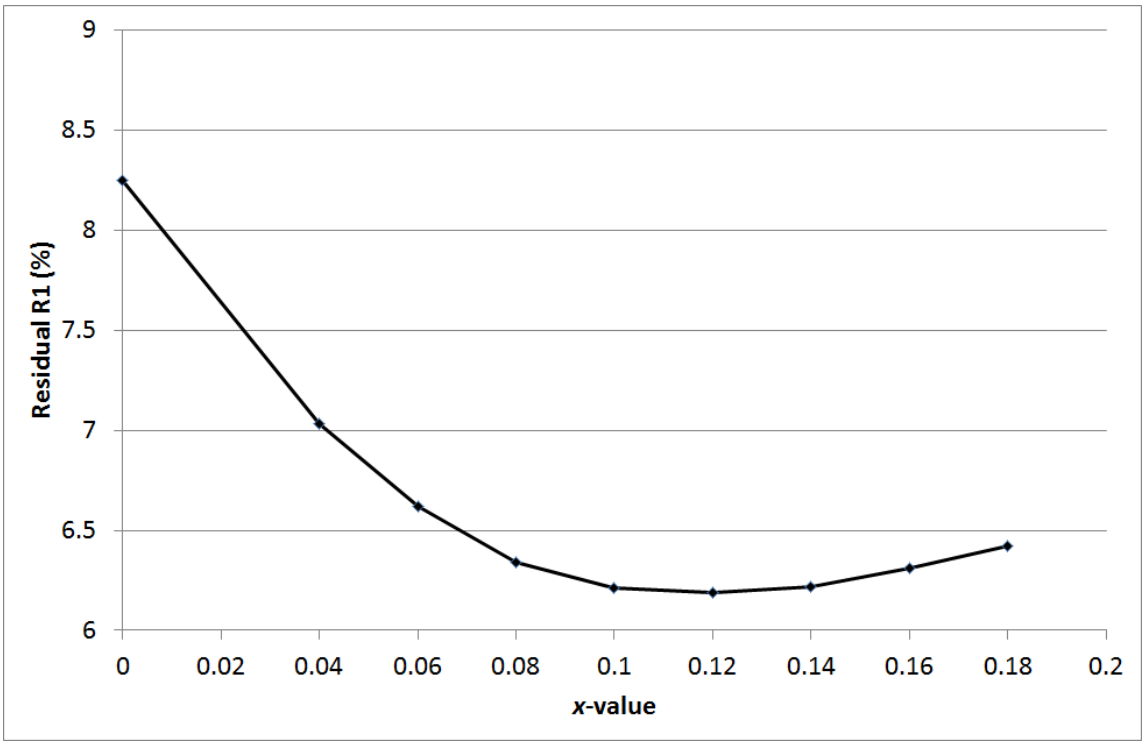


635

636 Fig. 5: Residual R1 plotted vs. *x*-value in $Al_{8+4x}Si_{4-4x}O_{20-2x}$.

637

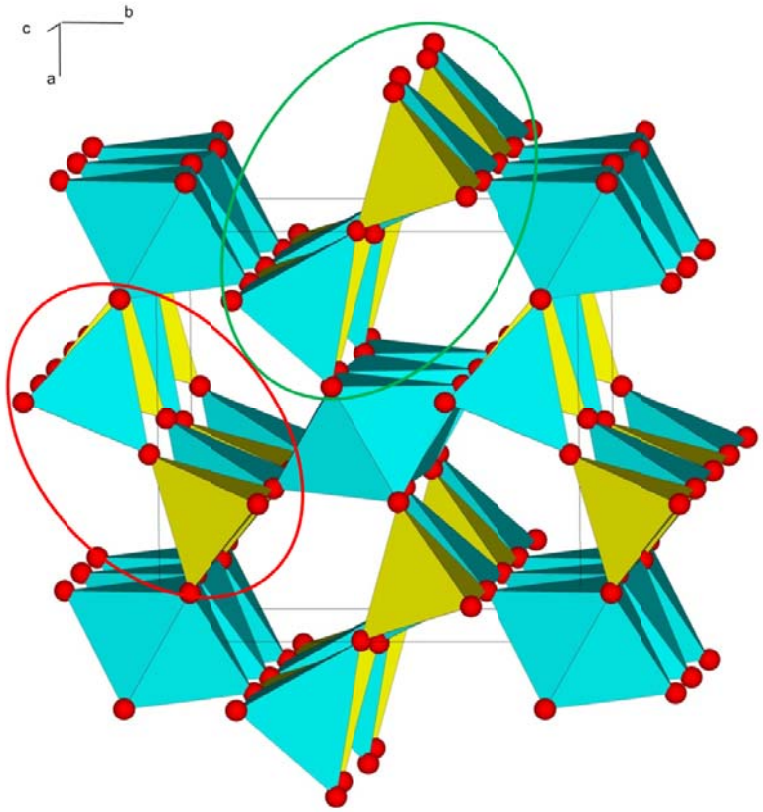


638

639 a) Sillimanite in space group *Pbnm* (Yang et al. 1997)

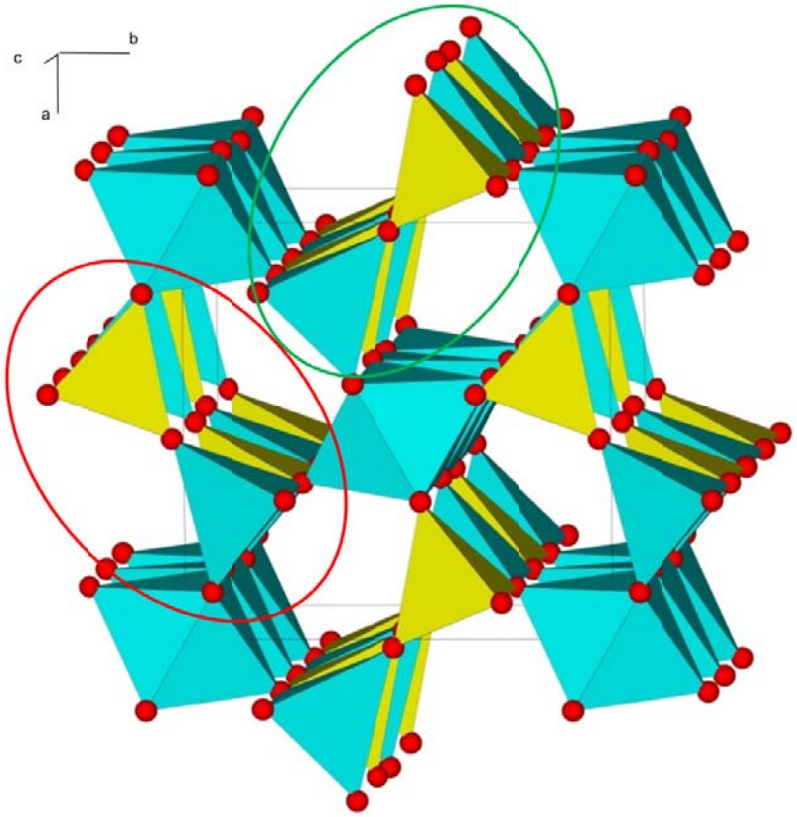


b) The crystal structure of „sillimullite“ in *Pnam*.

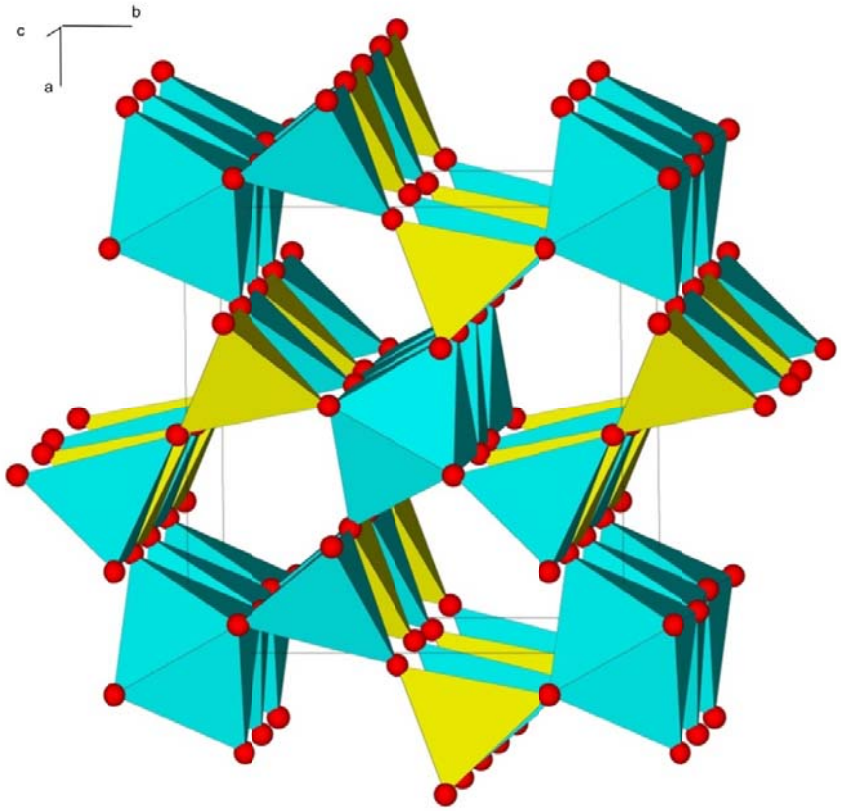


c) The crystal structure of „sillimullite“ transformed to *Pbnm* setting according to **b**, **a**, **-c**.

Fig. 6: Crystal structure projections of sillimanite and „sillimullite“ in the two space-group settings in an idealized representation ignoring oxygen vacancies and triclusters in „sillimullite“. Identical sequences of Si and Al in the tetrahedral double chains are encircled by a green oval and different sequences by a red oval. Neighboring double chains are shifted by ½ unit cell parallel to **c**. Blue polyhedra are occupied by Al, yellow ones by Si. View parallel to **c** rotated by 6° about **a** and **b**.

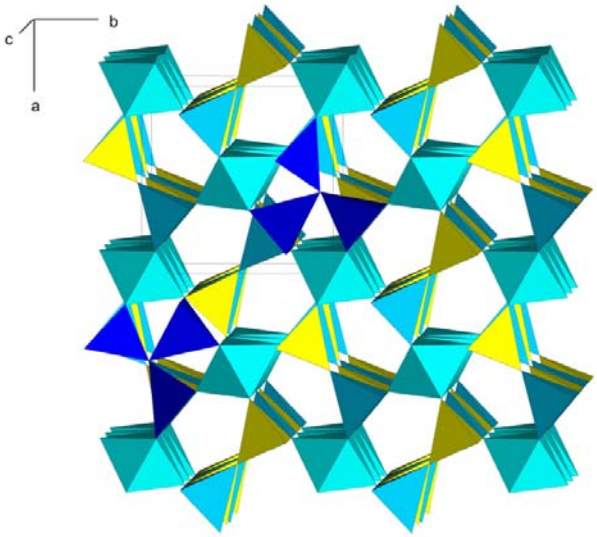


a) Representation of four unit cells. One is outlined in the upper left part.

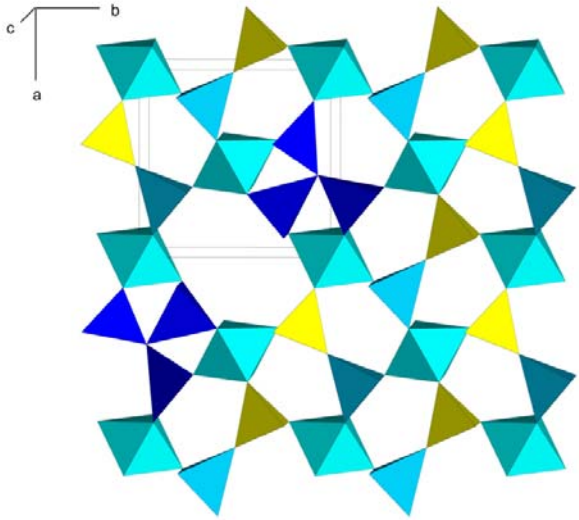


b) The upper layer with one oxygen vacancy.

Fig. 7: Crystal-structure projection of „sillimullite“ with an oxygen vacancy in 1, ½, 1. Triclusters consisting of two $TO_4$ and one $T^*O_4$ groups are dark blue. The colors of the other polyhedra correspond to those in Fig.6. O atoms are omitted for clarity. View parallel **c** rotated by 4° about **a** and **b**.

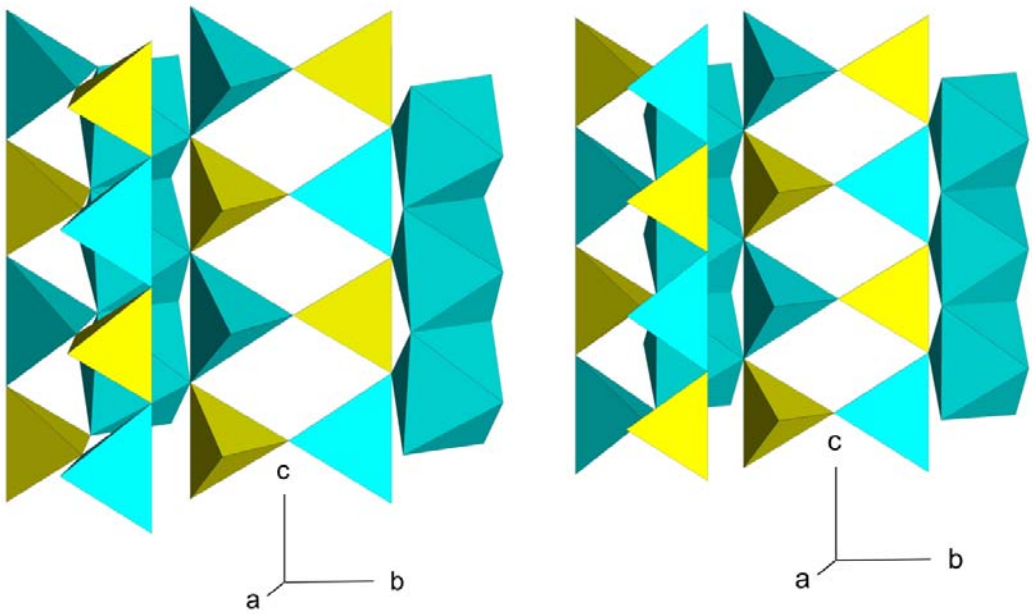


a) sillimanite b) „sillimullite“

Fig. 8: Crystal structure projections of the tetrahedral double chains in sillimanite and „sillimullite“. The right double chains correspond to the encircled chains in Fig. 6, the left double chains correspond to the chains in ½,0,*z* in Figs. 6a and b. Colors are assigned as in Fig. 6. View parallel a rotated by 20° about **c** and 5° about **b**. a) sillimanite. b) „sillimullite“.

675

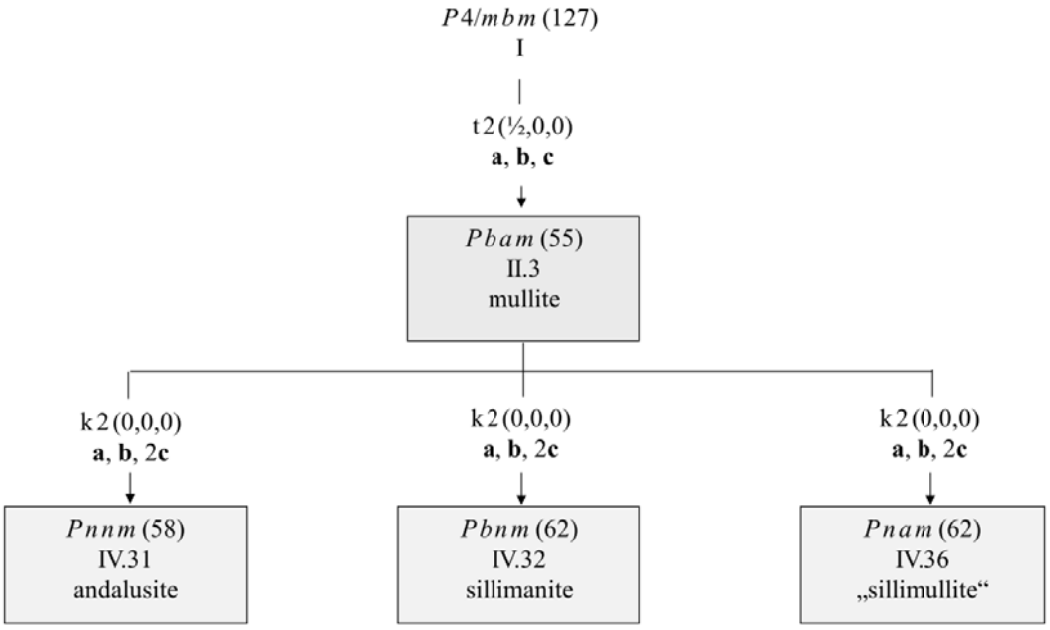


676

677 Fig. 9: The Bärnighausen tree illustrating the symmetry relationships of „sillimullite“ in
678 comparison to those of mullite, sillimanite and andalusite. The branches are derived from a
679 hypothetical aristotype representing the highest possible symmetry. Letters *t* and *k* represent
680 the type of symmetry reduction (*t* = translationengleich, *k* = klassengleich), followed by the
681 index (factor) of symmetry reduction and the origin shift in parentheses. Underneath, the set
682 of basis vectors is given which describes the transformation of a unit cell to its setting in the
683 subgroup. Space groups representing observed crystal structures are put in frames. Numbers
684 in parentheses behind the space-group symbol refer to the space-group number in the
685 International Tables for Crystallography (Hahn 2005). Roman numerals refer to the index of
686 symmetry reduction relative to the aristotype. Members on one level are distinguished by
687 Arabic numerals carrying the root numbers of the supergroup.
688

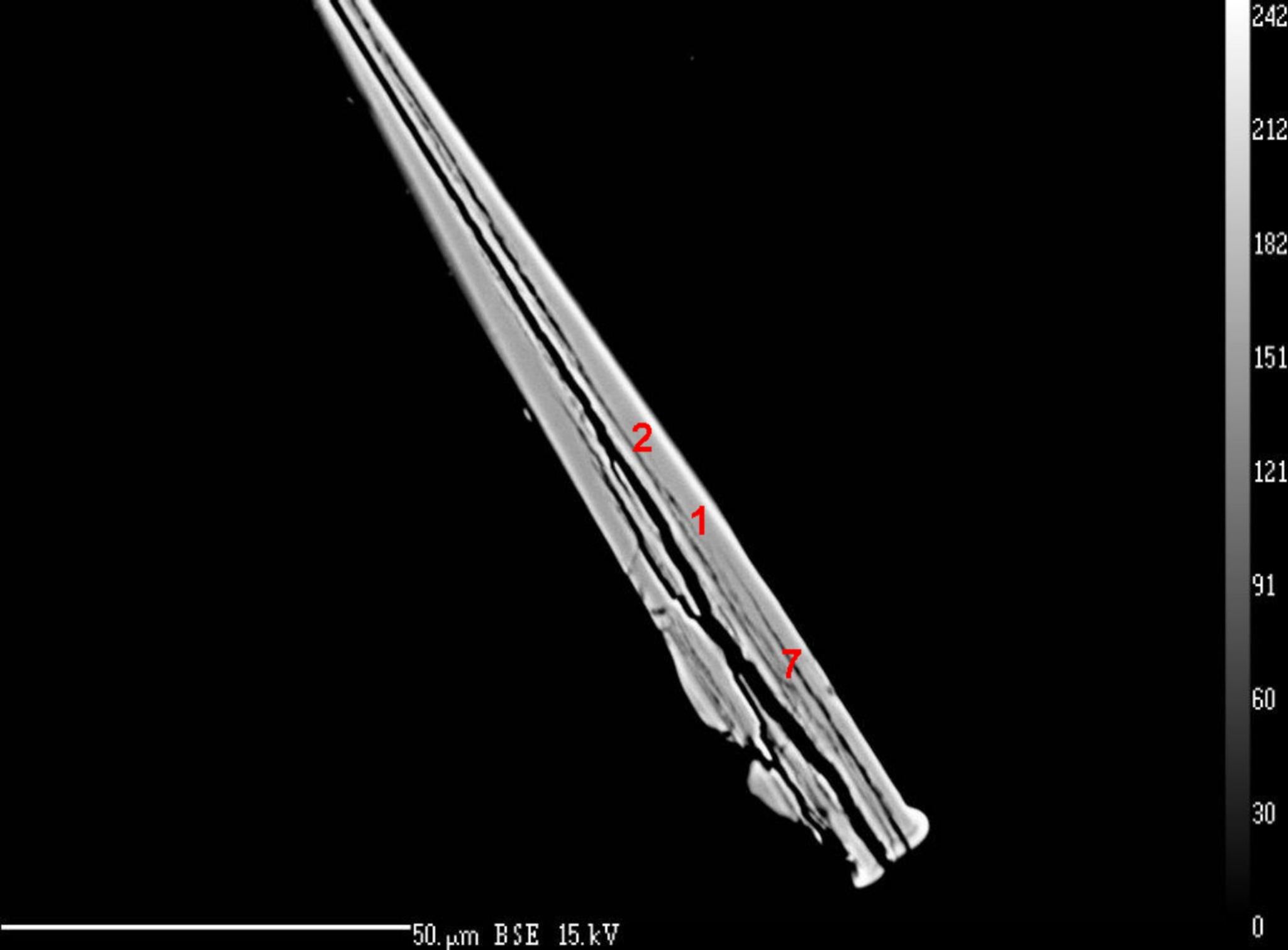
2
1
7
242
212
182
151
121
91
60
30
0
50.μm BSE 15.kV

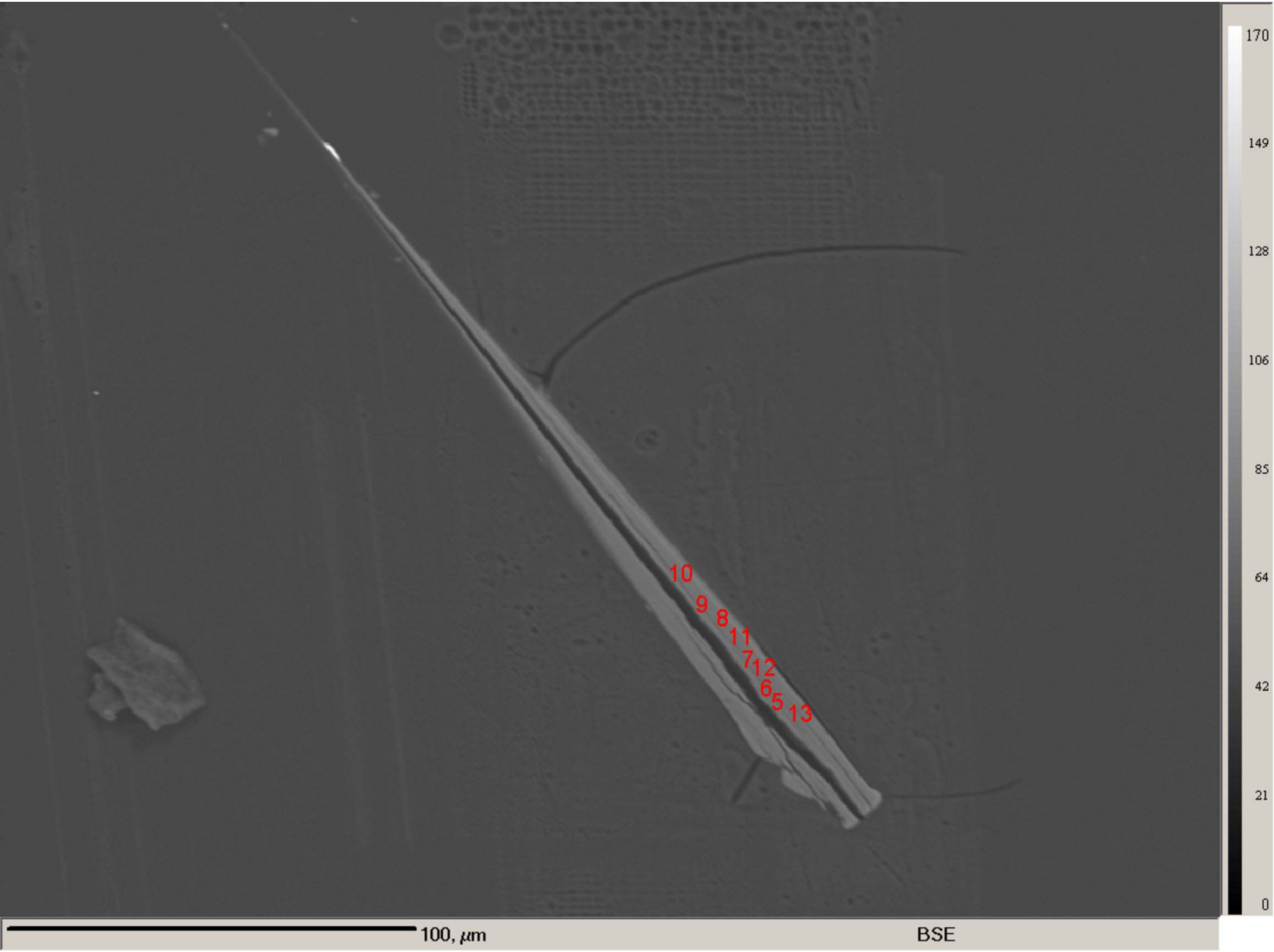
10
9
8
11
7
12
6
5
13
170
149
128
106
85
64
42
21
0
100, μm
BSE

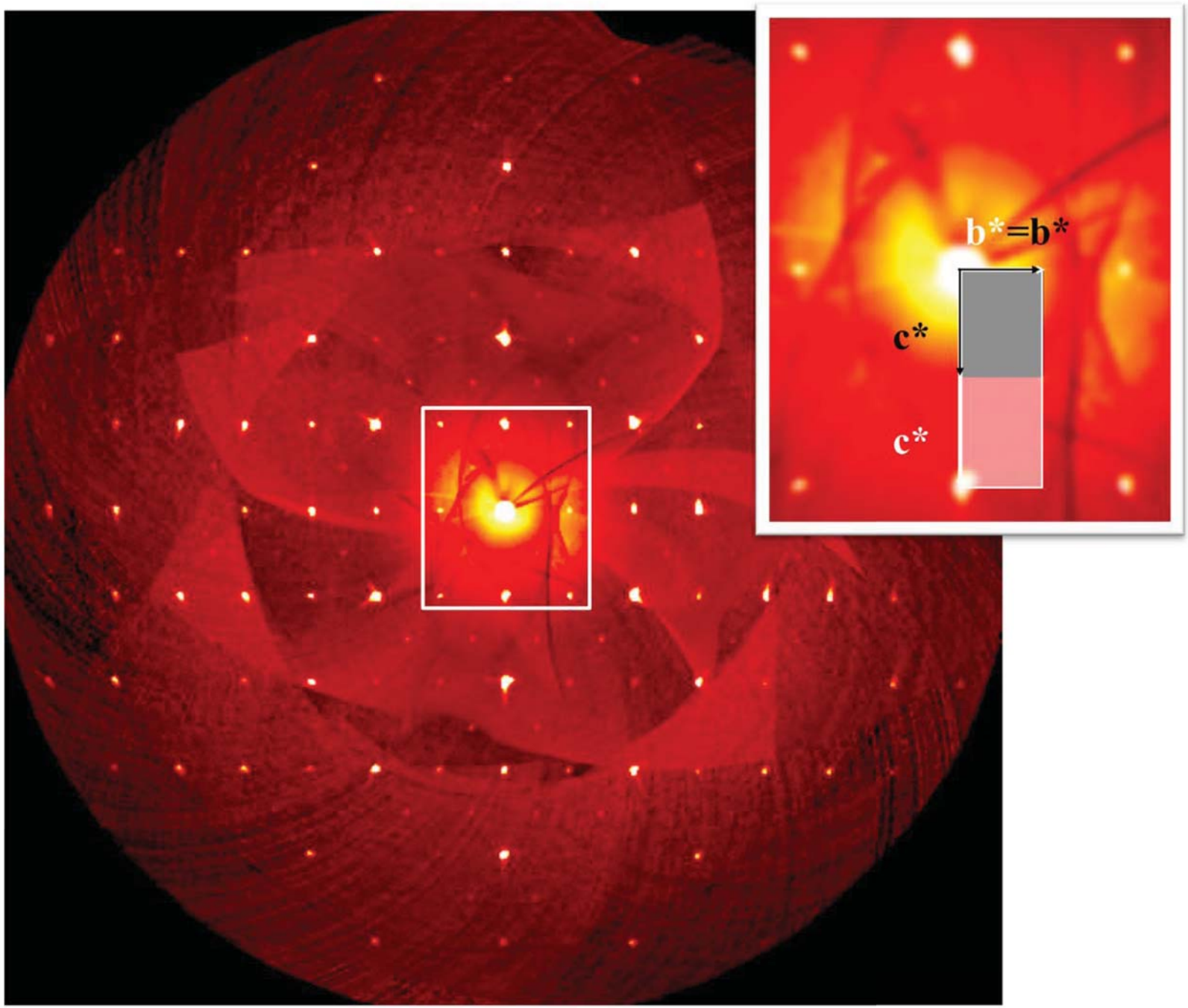
b*=b*
c*
c*

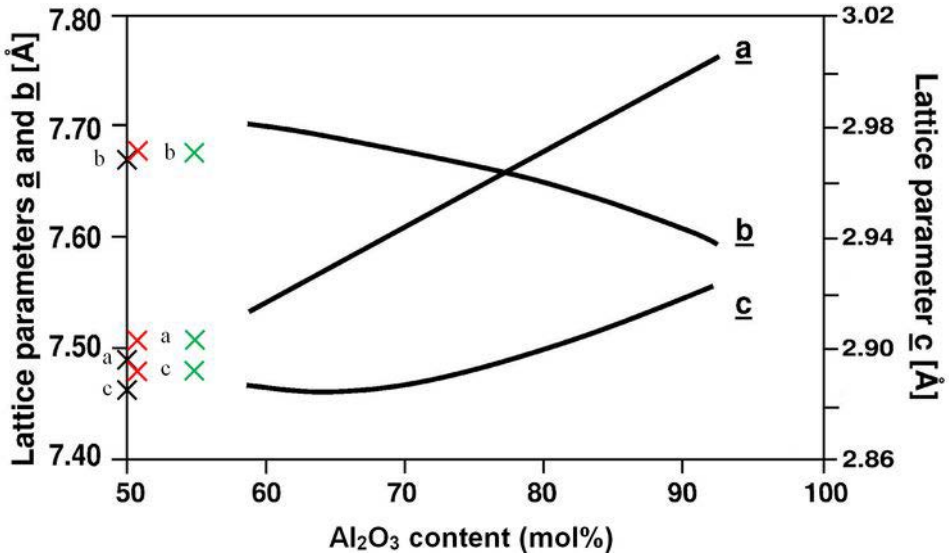
Lattice parameters a and b [Å]
Lattice parameter c [Å]
Al2O3 content (mol%)
7.80
7.70
7.60
7.50
7.40
3.02
2.98
2.94
2.90
2.86
50
60
70
80
90
100
a
b
c
b
b
a
a
c
c

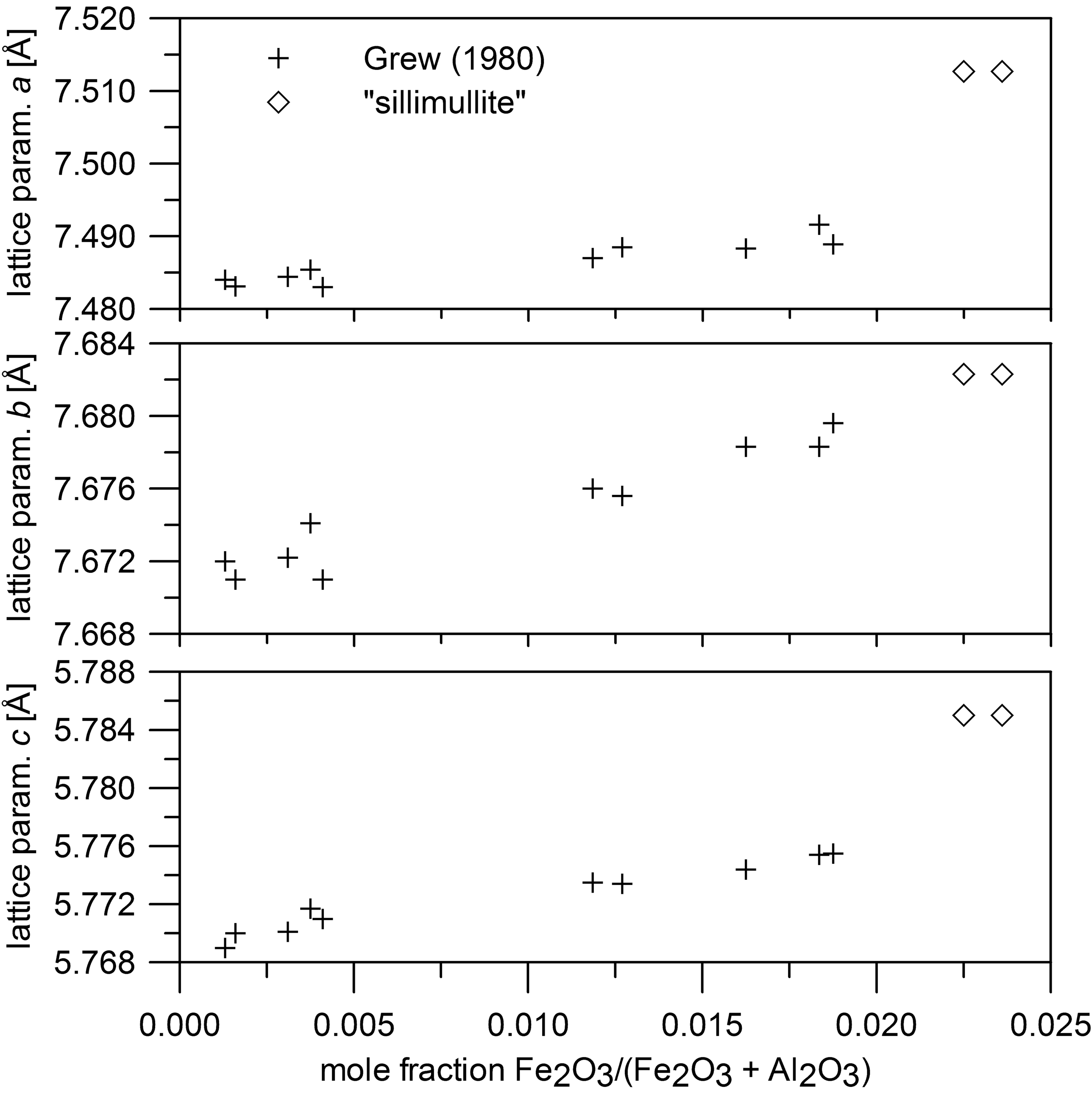
Grew (1980)
"sillimullite"
lattice param. a [Å]
7.520
7.510
7.500
7.490
7.480
lattice param. b [Å]
7.684
7.680
7.676
7.672
7.668
lattice param. c [Å]
5.788
5.784
5.780
5.776
5.772
5.768
0.000
0.005
0.010
0.015
0.020
0.025
mole fraction Fe2O3/(Fe2O3 + Al2O3)

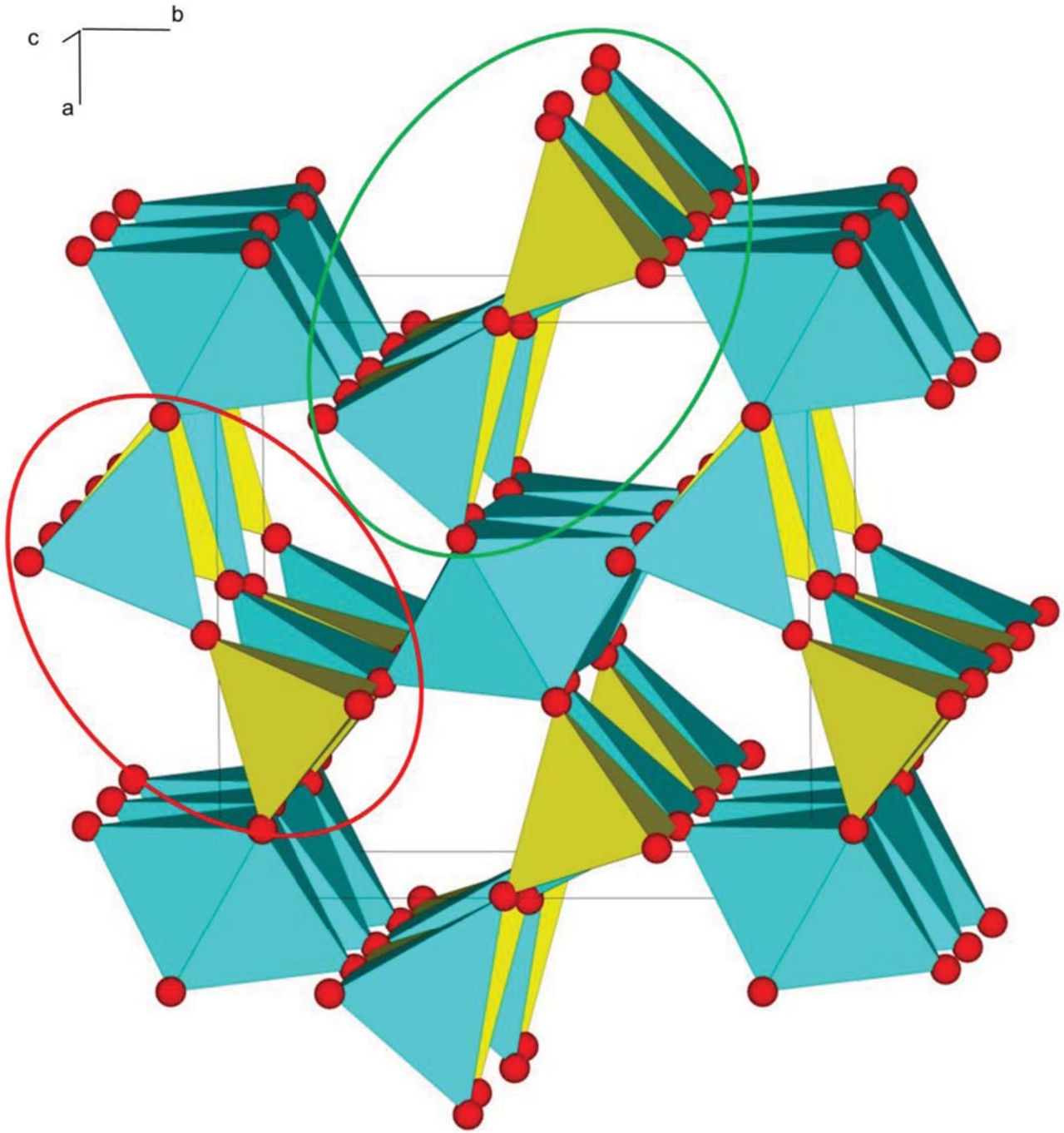
c
b
a

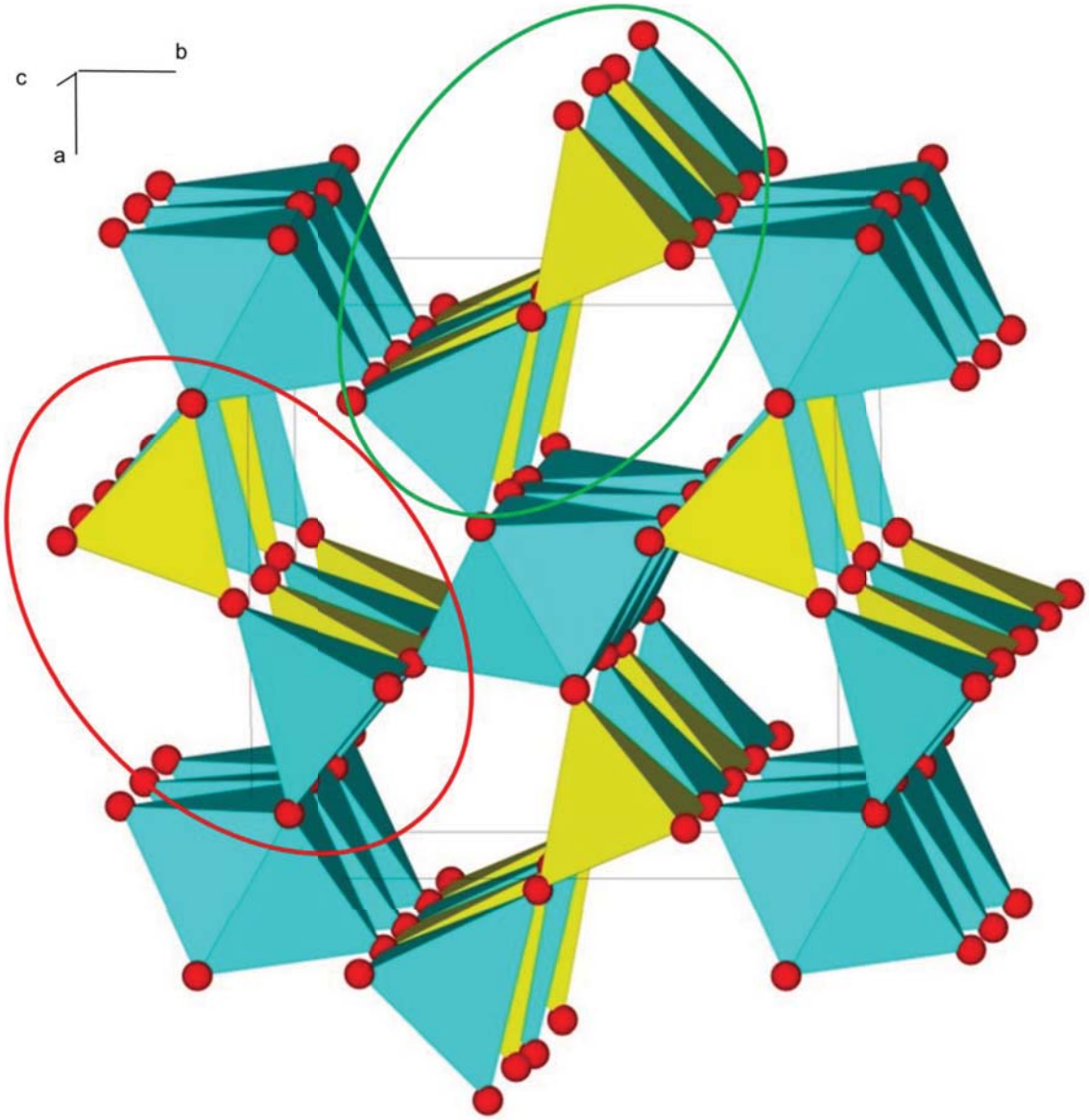
b
c
a

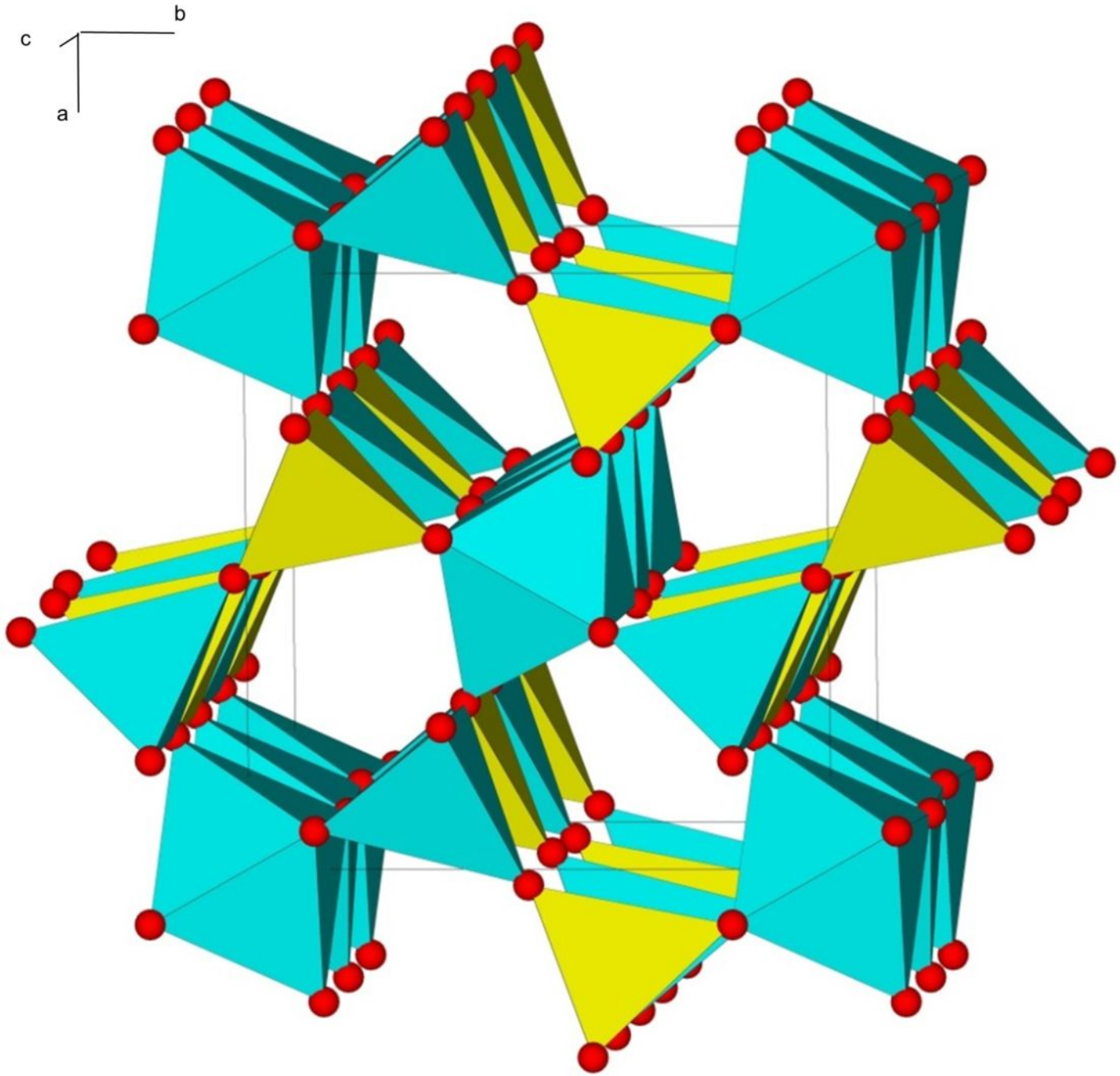
b
c
a

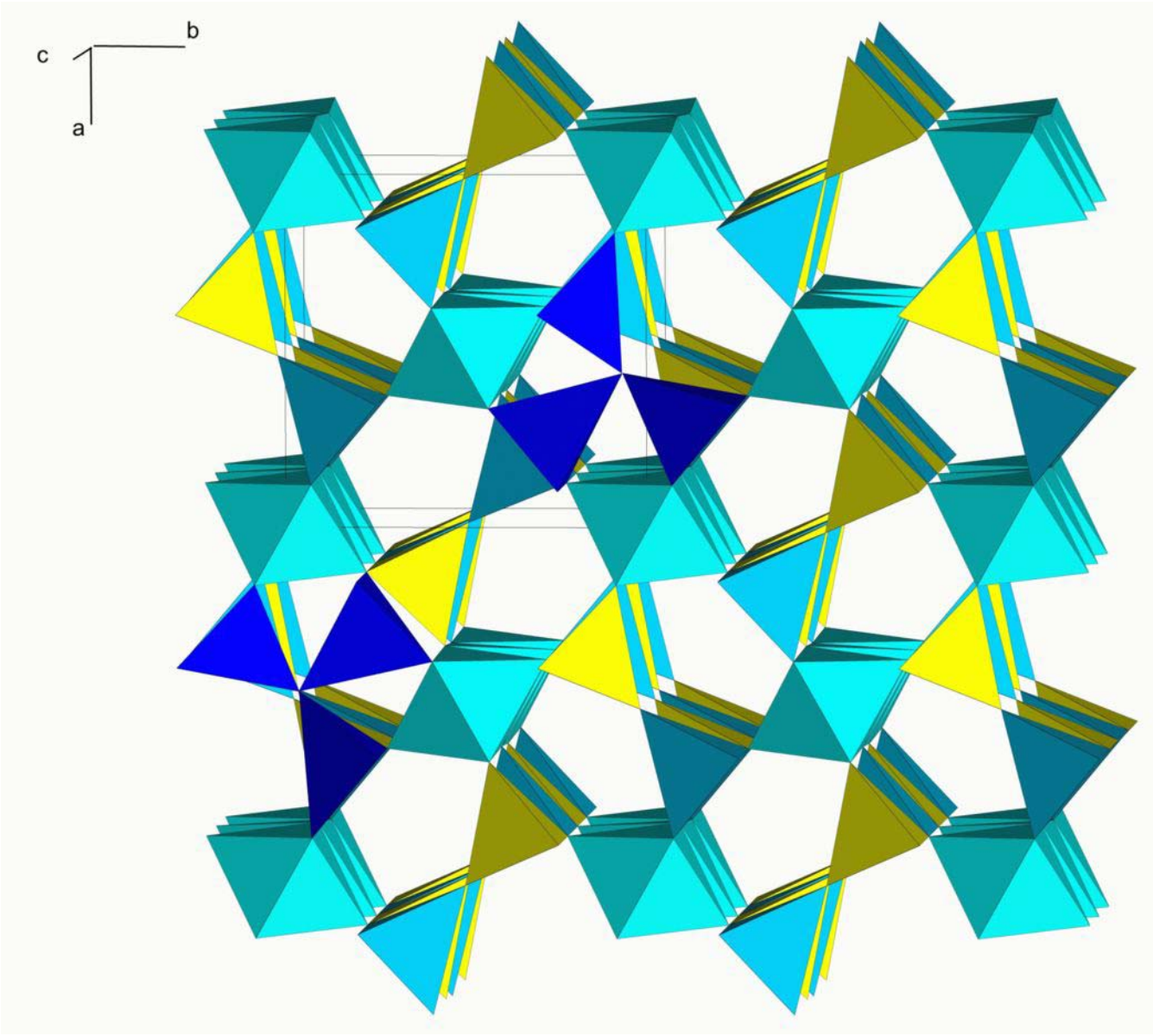
c
b
a

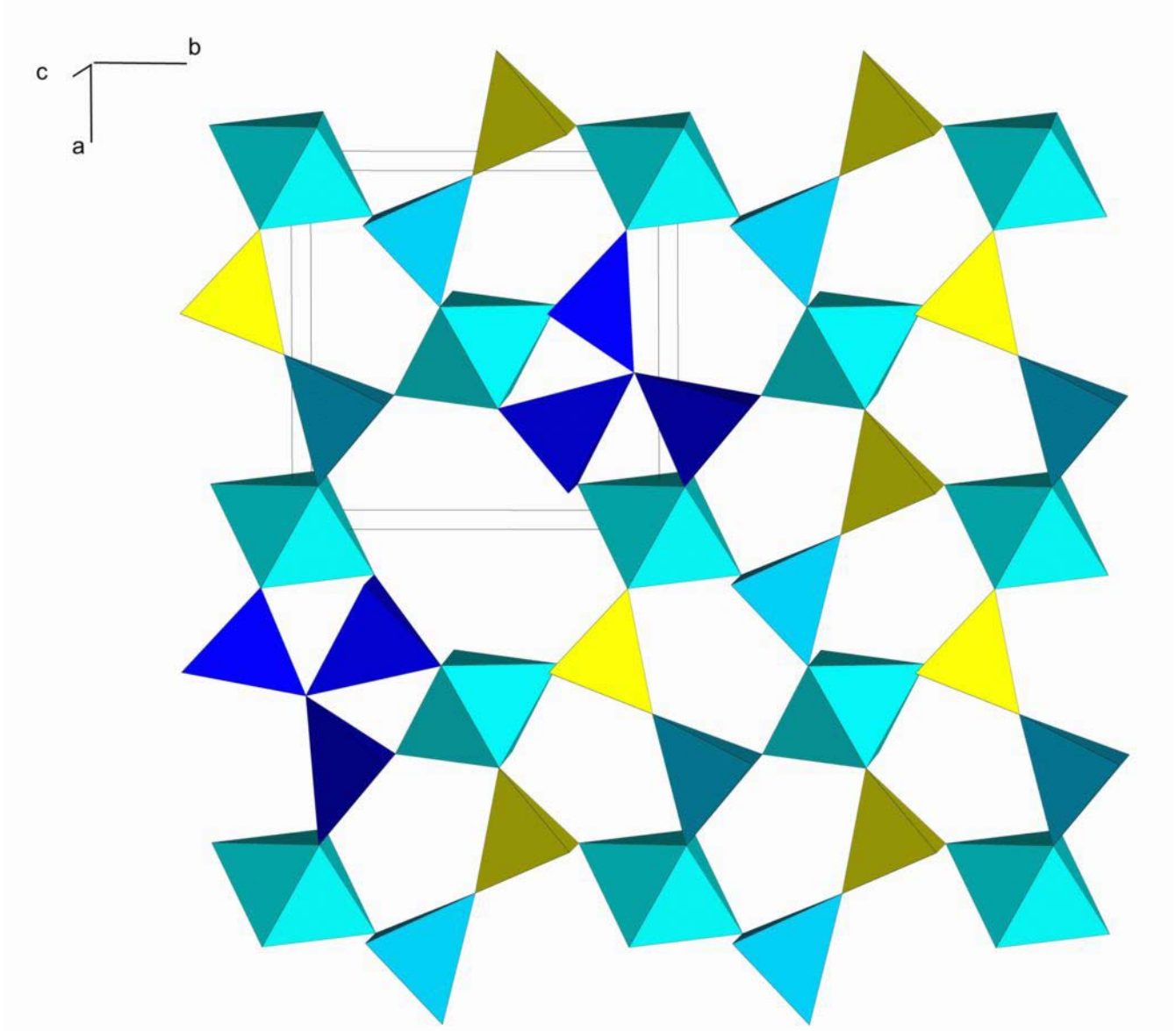
b
c
a

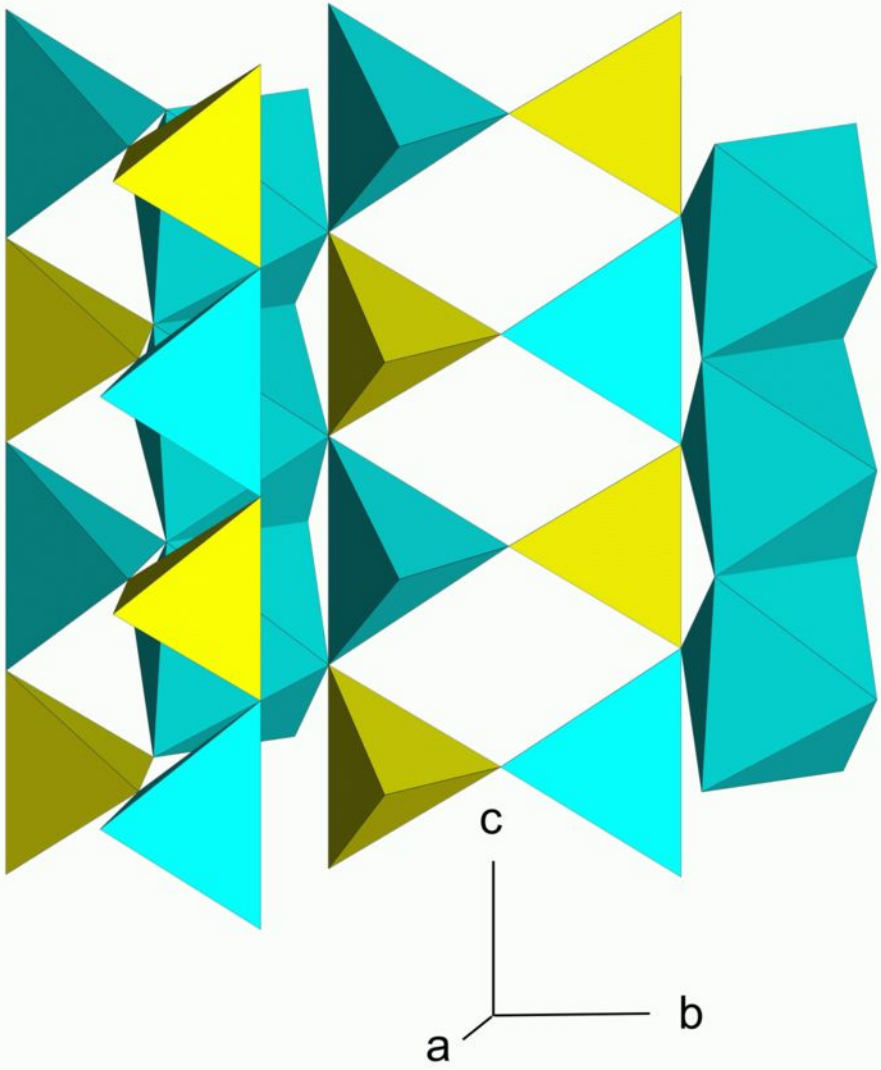
c
b
a

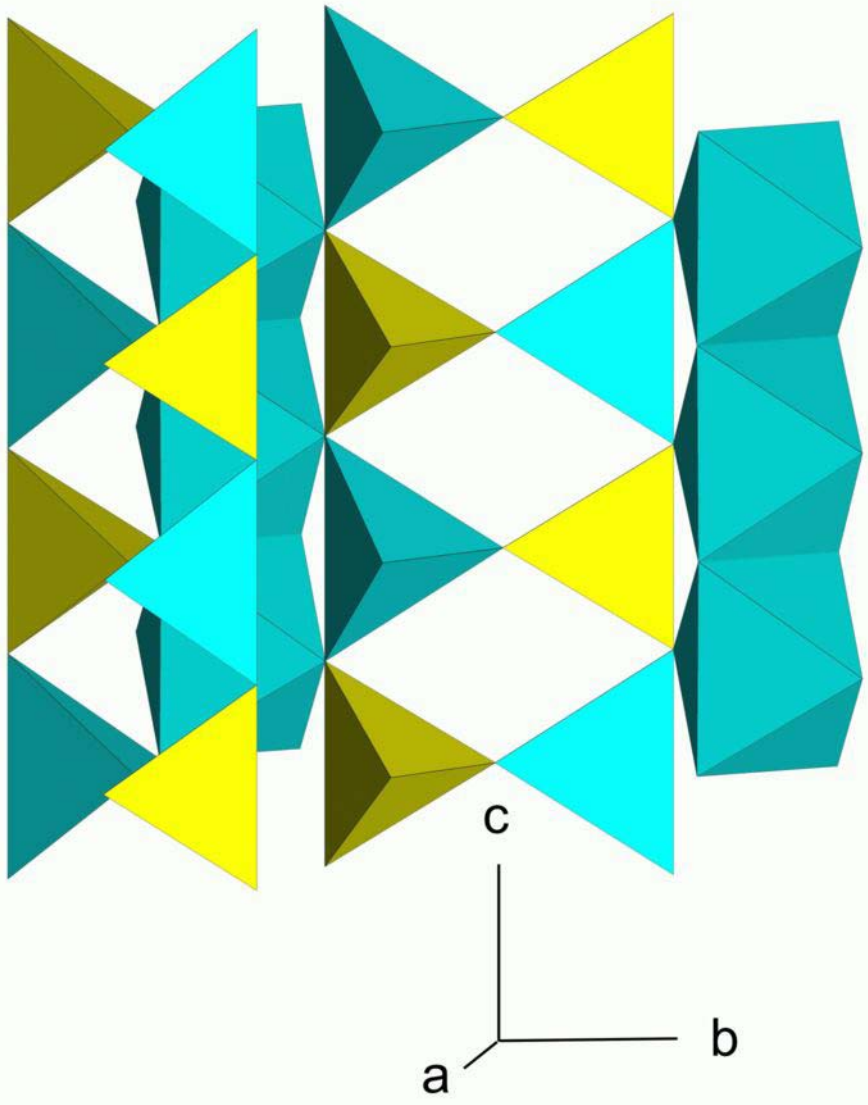
c
b
a